Notch signaling represses cone photoreceptor formation through the regulation of retinal progenitor cell states

Xueqing Chen[1,2], Mark M. Emerson[1,2,3*]

[1] Biology PhD Program, The Graduate Center, The City University of New York, New York, NY, 10016

[2] Department of Biology, The City College of New York, The City University of New York, New York, NY, 10031

[3] Biochemistry PhD Program, The Graduate Center, The City University of New York, New York, NY, 10016

*Corresponding author: memerson@ccny.cuny.edu

Email addresses:

Xueqing Chen: xchen2@gradcenter.cuny.edu

Mark Emerson: memerson@ccny.cuny.edu

Keywords: retinal progenitor cells, multipotency, cis-regulation, cone photoreceptors, Notch signaling, electroporation

Abstract

Vertebrate cone photoreceptor formation is a multistep process. First, multipotent retinal progenitor cells generate genetically-defined restricted/neurogenic progenitor cells and these cells then divide to preferentially produce cones and horizontal cells. Notch signaling represses cone formation and maintains the proliferative potential of retinal progenitor cells. However, the mechanisms through which it affects these processes are unknown. Here we use cell type specific inhibition of Notch signaling to localize the primary role of Notch signaling during cone genesis to the regulation of restricted retinal progenitor cells from multipotent retinal progenitor cells. Notch signaling inhibition in restricted progenitor cells does not alter the number of cones derived from these cells but does affect horizontal cell development. Cell cycle promotion is not a primary effect of Notch signaling but an indirect effect on progenitor cell state transitions that leads to depletion of the multipotent progenitor cell population. Taken together, this suggests that the roles of Notch in cone photoreceptor formation and cell cycle promotion are both mediated by a localized function in multipotent retinal progenitor cells to repress the formation of restricted progenitor cells.

Introduction

Notch signaling is an evolutionarily conserved signaling pathway that functions in diverse cellular contexts to drive both cell cycle and cell fate decisions. In canonical Notch signaling, extracellular binding of a member of the Delta/Serrate/Lag family of proteins to the extracellular portion of the transmembrane Notch receptor leads to a proteolytic cleavage that releases the Notch intracellular domain (NICD) from the membrane (Bray, 2006; Kopan and Ilagan, 2009). The NICD then translocates to the nucleus, and through a primary interaction with the MAML protein, forms a tripartite complex with the Rbpj transcription factor that affects transcription of target genes (Mumm and

Kopan, 2000; Wu et al., 2000). Notch signaling can act iteratively and participate in several distinct decisions that occur during the process of formation of a particular cell type. For example, during the formation of Drosophila sensory neurons from ectoderm, Notch signaling is critical in three successive cell fate decisions (Artavanis-Tsakonas et al., 1991; Bray, 1998).

Though the role of Notch signaling in cell fate decisions in Drosophila and C. elegans has been implicated in binary cell fate choices (Lai, 2004), the specific role of Notch signaling in the vertebrate nervous system has not been as clear. During the formation of the vertebrate retina, a functional role for Notch signaling in both proliferation and in cell fate choice has been identified. Induction of conditional loss-of-function alleles for the Notch1 receptor during early retinogenesis leads to cell cycle exit and increased cone photoreceptor formation (Jadhav et al., 2006; Yaron et al., 2006). In one of these studies, a loss of horizontal cells (HCs) was also described (Yaron et al., 2006). Similarly, conditional Rbpj loss-of-function increases the formation of cone photoreceptors while also promoting the formation of retinal ganglion cells (RGCs) (Riesenberg et al., 2009). In both cases, Notch1 and Rbpj loss-of-function leads to a decrease in proliferation. Conditional loss of Notch1 in the later postnatal period, after the window of cone genesis, reveals that rod photoreceptors are also increased, which suggests that Notch signaling plays a more general role in repression of the photoreceptor fate (Jadhav et al., 2006). In addition, it has been suggested in this postnatal context that Notch signaling can function in postmitotic cell fates to repress the rod fate (Mizeracka et al., 2013). Despite these significant advances, the mechanisms through which Notch affects these processes are still unknown and has implications for both visual system evolution and retinal therapy development.

While previous studies have implicated Notch signaling in the generation of cone and rod photoreceptors, it is not yet clear at which step in their formation that it acts. Recently, the formation of cones has been identified as a multistep process. During the early stages of retinal formation when cone

91 photoreceptors are preferentially generated, multipotent retinal progenitor
92 cells (RPCs) divide to form restricted (also known as neurogenic RPCs) RPCs
93 that can be identified by the activity of the ThrbCRM1 cis-regulatory element,
94 the expression of specific transcription factors (Otx2, OC1 and Olig2), and the
95 decreased expression of canonical RPC markers, such as Vsx2
96 (Buenaventura et al., 2018; Emerson and Cepko, 2011; Emerson et al., 2013;
97 Jean-Charles et al., 2018). These restricted RPCs lack the diverse cell fate
98 potential of the multipotent RPC and instead preferentially divide to form cone
99 and HCs as well as a minor number of RGCs (Cepko, 2014; Emerson et al.,
100 2013; Schick et al., 2019). Thus, Notch signaling could mediate cone genesis
101 through regulation of the multipotent to restricted RPC transition, the cell fate
102 choices of the restricted RPC daughter cells, or in the production of cones
103 directly from multipotent RPCs or other cell types.
104 In this study, we used defined cis-regulatory elements to both quantitate
105 the effects of Notch signaling inhibition and also to limit interference with
106 Notch signaling to specific cell types. We determined that during the formation
107 of cone photoreceptors, inhibition of Notch signaling specifically promoted the
108 formation of restricted RPCs from multipotent RPCs but did not promote the
109 cone fate in the daughter cells of restricted RPCs. As expected for such a shift
110 in cycling populations, there was minimal short-term effect on proliferation as
111 measured by EdU labeling. Taken together, this suggests that a primary role
112 of Notch signaling during cone photoreceptor genesis is to regulate the
113 formation of restricted RPC states from multipotent RPCs.
114

115 **Results**

116 **Evaluation of Notch reporter activity in response to MAML dominant-**
117 **negative**

118 To provide precise and rapid interference with Notch signaling, we used a
119 dominant-negative approach. We first created a chicken version of a
120 previously validated, and widely used, C-terminal truncation version of MAML

121 that retains the ability to interact with the Notch intracellular domain but lacks
122 the domains necessary to induce a transcriptional response (referred to as
123 MAML-DN) (Tan et al., 2016; Weng et al., 2003). The MAML1 gene was used,
124 as it was the MAML gene most highly expressed in the developing chicken
125 retina according to reported RNA-Seq data (Buenaventura et al., 2018). To
126 test the effectiveness of the MAML-DN construct, we used previously reported
127 Notch reporters Hes5::GFP (Vilas-Boas et al., 2011), Hes1::GFP (Mizutani et
128 al., 2007) and 12XCSL::EGFP (Hansson et al., 2006). Hes1 and Hes5 are two
129 previously used transcriptional reporters of Notch signaling derived from
130 characterized Notch target genes. The Hes1 gene is broadly expressed in
131 RPCs while the Hes5 gene is dynamic and expressed in RPCs and
132 differentiating retinal ganglion neurons (Riesenberg et al., 2018). The 12XCSL
133 reporter construct is a synthetic element composed of 12 multimerized Rbpj
134 motifs.

135 E5 chicken retinas were co-electroporated ex vivo with one of the Notch
136 GFP reporters, a ubiquitous electroporation control (CAG::Nucßgal), and with
137 or without the MAML-DN construct. After two days of culture, retinas were
138 imaged by confocal microscopy or analyzed by flow cytometry (Fig. 1A). In
139 control retinas, the Hes1::GFP reporter was broadly distributed across the
140 retina and appeared to be in the majority of targeted cells (Fig. S1). This
141 pattern was unexpected for a Notch reporter given the enriched expression of
142 Notch in RPCs and the restricted expression of Hes1 expression. In addition,
143 the Hes1::GFP reporter activity levels did not appear to be affected by MAML-
144 DN expression (Fig. S1). In contrast, the Hes5::GFP reporter was active
145 primarily in the neuroblast layer of the retina, where multipotent RPCs are
146 located, and the reporter activity was drastically abrogated in response to
147 MAML-DN introduction (Fig. 1B). The 12XCSL::EGFP reporter showed low
148 expression levels in targeted cells, however, MAML-DN also decreased this
149 reporter (Fig. S1). Strikingly, we found in all the experimental groups that the
150 retinal distribution of the electroporated population was altered, with cells

151 found predominantly in the scleral region where photoreceptor cells and
152 Otx2/OC1+ RPCs are enriched, as well as the RGC layer, but not in the
153 middle portion of the retina where most multipotent RPCs are localized (Fig.
154 1B) (Buenaventura et al., 2018). This suggested that there could be cell fate
155 changes in response to the MAML-DN mutant.

156 To quantify Notch reporter activity, we used a flow cytometry assay and
157 calculated the percentage of GFP-positive cells within the electroporated cell
158 population (Fig. 1C). The quantification supported the conclusions of the
159 confocal imaging results, as Hes5::GFP reporter activity showed a significant
160 decrease in response to MAML-DN introduction. We also confirmed the
161 effects of inhibited Notch signaling using dominant-negative forms of Rbpj
162 (Rbpj-EnR), in which the full-length Rbpj was fused with an engrailed
163 repressor at either the N-terminus or C-terminus and co-electroporated with
164 the same Notch reporters. Hes5 reporter activity significantly decreased in the
165 presence of both dominant-negative constructs (Fig. 1C and Fig. S2). In
166 summary, the Notch reporter Hes5::GFP displayed the most robust readout of
167 Notch signaling activity in this developmental context and the MAML-DN and
168 Rbpj-EnR constructs were all effective at inhibiting Notch signaling as gauged
169 by the Hes5 reporter.

170

171 **Inhibition of Notch promotes the formation of restricted progenitor cells**

172 A mouse knockout of the Notch1 receptor leads to an increase in cone
173 photoreceptors (Jadhav et al., 2006; Yaron et al., 2006), but the mechanism
174 behind this phenotype is unknown. One possibility is that in the knockout,
175 multipotent RPCs produce more of the RPC type that is restricted to cone and
176 HC fates, which in turn divide to form cones. The cis-regulatory element
177 ThrbCRM1 provides a robust tool to answer the question as it is active
178 specifically in this restricted RPC type (Emerson et al., 2013).

179 We first tested the effect of Notch inhibition in retinal development using
180 DNA reporters, including reporters with enrichment in multipotent RPCs

181 (VSX2ECR4; Buenaventura et al., 2018), cone/HC restricted RPCs
182 (ThrbCRM1; Emerson et al., 2013), subsets of cones (ThrbCRM2; Emerson et
183 al., 2013; Schick et al., 2019) and HCs/RGCs (OC1ECR22; Patoori et al.,
184 2020 and manuscript in preparation). E5 chicken retinas were electroporated
185 with a co-electroporation control, with or without the MAML-DN, and assessed
186 by confocal microscopy after two days culture. In retinas in which MAML-DN
187 was introduced, the number of ThrbCRM1 reporter-labeled restricted RPCs
188 was visibly increased, while the number of VSX2ECR4-labeled multipotent
189 RPCs was decreased and presented with altered morphology (Fig. 2A). The
190 number of ThrbCRM2 reporter-labeled cones and OC1ECR22 reporter-
191 labeled HCs/RGCs were qualitatively unchanged at this timepoint (Fig. S3).
192 The quantification of these cell types using flow cytometry statistically
193 confirmed these effects (Fig. 2B). This suggested that the broad inhibition of
194 Notch signaling via CAG::MAML-DN promotes the formation of ThrbCRM1-
195 active restricted RPCs. The down-regulation of VSX2ECR4 reporter-positive
196 RPCs, and significantly increased number of VSX2ECR4/ThrbCRM1 double
197 reporter-positive RPCs (Fig. 2B), suggests a transition from multipotent RPCs
198 to ThrbCRM1-positive RPCs in CAG::MAML-DN mutant retina. Intriguingly,
199 ThrbCRM2-labeled cones did not significantly increase after 2 days culture,
200 which could indicate a delay in cone genesis at this time point.
201 The increase in ThrbCRM1 reporter-positive cells could be due to an
202 increase in the ThrbCRM1 state, but it could also represent an increase in
203 their daughter cell production (cones, HCs, or RGCs) that could be missed by
204 the specific reporters used (Schick et al., 2019). We first examined Otx2 and
205 Visinin expression to confirm the reporter-observed effects, as these
206 endogenous markers are expressed in both photoreceptors and restricted
207 RPCs (Buenaventura et al., 2018; Emerson et al., 2013). In retinas with
208 introduction of the CAG::MAML-DN construct, there was a significant increase
209 of electroporated Visinin and Otx2-labeled cells, consistent with the reporter
210 results (Fig. 3A, B). Assessment of Olig2 expression, which is expected to be

211 expressed in ThrbCRM1-labeled RPCs and not cones or HCs, was
212 significantly increased, which suggests that the ThrbCRM1 reporter-positive
213 population observed at this 2 day period represents the restricted RPC state
214 (Fig. 3A and 3C) (Emerson et al., 2013; Ghinia Tegla et al.; Hafler et al.,
215 2012). In alignment with this observation and the ThrbCRM2 reporter result,
216 expression of the cone gene Lhx4 was not qualitatively changed (Fig. S3)
217 (Buenaventura et al., 2019). In contrast, the representation of the H1 HC
218 population (marked by Lim1 and AP2α; Fischer et al., 2007) that is normally
219 generated by ThrbCRM1 restricted RPCs is decreased in response to
220 CAG::MAML-DN (Figure 3B). No significant changes in the H2-4 HC/RGC
221 marker Isl1 or the Brn3 family of RGC markers were observed (Fig. S4)
222 (Fischer et al., 2007; Liu et al., 2000). Taken together, these data suggest that
223 the primary effect of Notch inhibition at this timepoint is to increase the
224 formation of the restricted RPCs that generate cones and HCs.
225 To further validate that these MAML-DN effects were related to Notch
226 signaling, we used flow cytometry to assess the effects of dominant-negative
227 forms of Rbpj on these same DNA reporters and cell markers. Similar effects
228 were observed upon introduction of both Rbpj-EnR constructs in support of a
229 basis in Notch signaling (Fig. S5). However, it was observed that the
230 reduction of HCs in response to the Rbpj-EnR constructs was more severe
231 than with MAML-DN, which is consistent with a Notch-independent role for
232 Rbpj to function in a complex with Ptf1a, a known regulator of HC genesis
233 (reviewed in Johnson and MacDonald, 2011).
234
235 **Notch inhibition does not affect the number of cones produced from**
236 **restricted RPCs**
237 To test whether MAML-DN also induces a shift from HCs to cones within
238 ThrbCRM1 reporter-positive RPCs, we replaced the ubiquitous CAG promoter
239 upstream of MAML-DN with the ThrbCRM1 specific enhancer, so that MAML-
240 DN would only be expressed in ThrbCRM1-active restricted RPCs. In contrast

241 to CAG::MAML-DN, introduction of this ThrbCRM1::MAML-DN into E5 retinas
242 did not alter the number of ThrbCRM1::GFP labeled RPCs. This suggests that
243 the ectopic ThrbCRM1 cells observed with the CAG promoter are not due to
244 induction of increased proliferation within the ThrbCRM1 population. Instead,
245 this supports a role for Notch in the multipotent RPC population, in which the
246 ThrbCRM1 element is not active (Fig. 4B).
247 To genetically maintain labeling in post-mitotic daughter cells, we used a
248 lineage tracing strategy to identify the retinal cells that have a ThrbCRM1
249 history (Fig. 4A) which were previously shown to be predominantly cones and
250 H1 HCs (Schick et al., 2019). A driver plasmid was used in which the PhiC31
251 recombinase is transcriptionally regulated by the cis-regulatory element
252 ThrbCRM1. In the responder plasmid, there is a STOP codon between a
253 broadly active CAG promoter and GFP, which is flanked by two recombinase
254 target sites. Excision of the STOP sequence upon ThrbCRM1-driven
255 expression of PhiC31 recombinase, will lead to GFP expression in cells with a
256 history of ThrbCRM1 activity (Schick et al., 2019).
257 The lineage tracing plasmids were introduced into the E5 retina, and then
258 the percentage of cones and HCs within the GFP-labeled retinal cells was
259 quantified using flow cytometry after two days culture. Intriguingly, the number
260 of cone photoreceptors did not change, as assessed by the expression of
261 Visinin and Otx2, while the percentage of Lim1 and AP2α-labeled HCs was
262 reduced (Fig. 4C and 4D). A small percentage of Isl1-labeled HCs and Brn3-
263 labeled RGCs are formed from ThrbCRM1 restricted RPCs, and no significant
264 changes in the populations were detected through cell counting in response to
265 introduction of the ThrbCRM1::MAML-DN (Fig. S6). Thus, the observed
266 reduction in HCs did not correspond to increased formation of cone
267 photoreceptors or Isl1-labeled HCs and RGCs in the daughter cell population
268 of ThrbCRM1 restricted RPCs. These unidentified cells potentially become
269 other cell types that cannot be identified by the cell markers used.
270

271 **Effects of MAML-DN on retinal cell proliferation and multipotency**

272 Previous analysis of mouse Notch1 conditional knockout retinas identified
273 a reduction in BrdU-positive cells, which suggested that loss of Notch
274 signaling promoted premature cell cycle exit and down-regulation of cell
275 proliferation (Jadhav et al., 2006; Yaron et al., 2006). However, the difference
276 in the percentages of BrdU-positive cells in wild-type and Notch1 CKO mutant
277 is relatively small. To investigate the role of Notch in retinal cell proliferation,
278 we co-electroporated CAG::MAML-DN and CAG::TdT into E5 chick retinas
279 and after two days culture pulsed with EdU for 1 hour to label proliferating
280 cells. We first quantified the percentage of EdU/CAG::TdT double-positive
281 cells in all the electroporated cells using flow cytometry. Intriguingly, the
282 population of proliferating cells does not significantly change compared to the
283 control (Fig. 5A). Introduction of the Rbpj dominant-negative construct
284 resulted in similar effects on electroporated EdU-positive cells (Fig. S7).

285 These data suggest that Notch signaling does not directly control cell
286 proliferation in retina. Although inhibition of Notch does not drastically alter the
287 overall number of RPCs within this timeframe, the experiments described
288 above suggest that it causes a shift from multipotent RPCs to restricted RPCs
289 with a significant increase in ThrbCRM1-positive RPCs, a reduction of
290 VSX2ECR4-positive RPCs, and a large increase in the number of
291 ThrbCRM1/VSX2ECR4 double reporter-positive cells (Fig. 2B). To confirm
292 that these identified populations are indeed proliferating, we co-electroporated
293 ThrbCRM1 and VSX2ECR4 reporters and pulsed with EdU just prior to
294 harvest to label RPCs. Flow cytometry was used to quantify the
295 EdU/ThrbCRM1 and EdU/VSX2ECR4 double-positive cells in the
296 electroporated population. We also measured the percentage of
297 EdU/ThrbCRM1/VSX2ECR4 triple-positive cells versus the combination of
298 EdU/ThrbCRM1 and EdU/VSX2ECR4 double-positive cells (Fig. 5B and 5D).
299 There was a significant up-regulation of ThrbCRM1+/EdU+ cells as well as
300 ThrbCRM1+/VSX2ECR4+/EdU+ cells that indicated a transition from

301 VSX2ECR4-active RPCs to ThrbCRM1-active RPCs within the EdU+
302 population (Fig. 5C). In addition, immunostaining with the ThrbCRM1 marker
303 Otx2 and the multipotent RPC marker VSX2 showed a down-regulation of
304 VSX2+/EdU+ cells and an up-regulation of Otx2+/EdU+ cells, validating a shift
305 between VSX2+ RPCs and ThrbCRM1-active RPCs (Fig. S8).
306 To further determine if the induced ThrbCRM1 RPCs were derived from
307 multipotent RPCs, we used the VSX2ECR4 element that is active in this
308 population to drive expression of PhiC31 recombinase and conduct lineage
309 tracing of this population. The number of VSX2ECR4/ThrbCRM1 double
310 reporter-positive cells increased 5-fold in response to CAG::MAML-DN (Fig.
311 5E). This increase was consistent with the majority of new ThrbCRM1
312 reporter-positive cells being derived from multipotent RPCs, which suggests
313 that Notch inhibition specifically affects the transition from the multipotent to
314 restricted RPC state.
315
316 **Temporal parameters of the transition from multipotent RPCs to**
317 **restricted RPCs**
318 We were interested in determining the timeframe with which multipotent
319 RPCs transition to restricted RPCs. To test if the changes in multipotent RPC
320 numbers could be detected during their first cell cycle after electroporation, we
321 electroporated E5 chick retinas with VSX2ECR4::GFP, ThrbCRM1::TdT, the
322 co-electroporation reporter CAG::iRFP, and either CAG::MAML-DN or control
323 conditions. Retinas were harvested at 8 hours after electroporation, which is a
324 time before multipotent RPCs would be expected to complete one cell cycle.
325 There were no significant differences in the number of VSX2ECR4-marked
326 multipotent RPCs or ThrbCRM1-marked restricted RPCs (Fig. 6A). In
327 addition, the VSX2ECR4/ThrbCRM1 double reporter-positive cells were
328 present in a very low level as observed in wild type in both MAML-DN and
329 Rbpj-EnR mutants (Fig. 6B and Fig. S7). After 20 hours culture, the
330 ThrbCRM1-active population started to increase slightly but not nearly as

331 much as observed after two days (Fig. 6C). However, the transition from
332 multipotent RPCs to restricted RPCs showed a small but significant up-
333 regulation, as the VSX2ECR4/ThrbCRM1 double reporter-positive cells
334 increased (Fig. 6C). Examination of Otx2 and VSX2 endogenous markers
335 revealed a more robust response, with a decreased VSX2-positive population
336 and an increased Otx2-positive one after 20 hours culture (Fig. 6D). Taken
337 together, these data suggest that the Notch inhibition transition did not occur
338 at 8 hours post-electroporation, but could be detected after 20 hours, and
339 increased further at 2 days post-electroporation. This suggests that
340 multipotent RPCs do not immediately transition to a restricted RPC state, but
341 do so after a delay that could be accounted for by a required progression
342 through a single, or multiple rounds, of cell division.
343
344 **Increased cone genesis in response to Notch inhibition is delayed**
345 **relative to restricted RPC formation**
346 While multiple experiments support the conclusion that Notch inhibition
347 leads to the formation of an increased restricted RPC population, we did not
348 detect any increased cone genesis within a 2-day post-electroporation window
349 (Fig. 2B and Fig. S3). To investigate the possibility that there is a delay in
350 cone genesis that will occur from the induced cone/HC RPCs, we used a
351 lineage tracing strategy to follow the fates of multipotent RPCs and assessed
352 the cone fate within this population. Chick retinas were electroporated with a
353 VSX2ECR4::PhiC31 lineage tracing plasmid, a GFP lineage tracing reporter,
354 a ThrbCRM2::TdTomato reporter, and CAG::iRFP to mark all electroporated
355 cells (Fig. 7A). Retinal samples were harvested after two to five days culture.
356 The total number of ThrbCRM2 reporter-positive cones did not change at 2 or
357 3 days post-electroporation, however, the number of ThrbCRM2 reporter-
358 positive cells within the VSX2ECR4 lineage-traced population showed a
359 significant increase at 3 days, in line with the hypothesis that the effects of
360 Notch inhibition originate from multipotent RPCs (Fig. 7B). Both the overall

361 ThrbCRM2 population and the population specifically lineage-traced from
362 multipotent RPCs showed a very significant enrichment at 4 and 5 days after
363 electroporation (Fig. 7C), which correlated in a delayed manner with the
364 changes of ThrbCRM1 restricted RPCs from 1 to 2 days (Fig. 6C and Fig.
365 2B). This supports our hypothesis that increased cone genesis has a delay of
366 2 days relative to the up-regulated ThrbCRM1 RPCs formed in response to
367 Notch inhibition and that this increased cone cell number is ultimately caused
368 by effects that originate in multipotent RPCs.
369

370 **Discussion**

371 While critical gene regulators of retinal cell type formation have been
372 identified in the last decades, the relationships of these factors within gene
373 regulatory networks and the cellular events in which they function are much
374 less clear. One of the primary reasons for this is that, unlike other
375 developmental systems, strict lineages of cell types originating from
376 multipotent RPCs have not been identified, leading to some hypotheses that
377 this system is driven primarily by stochastic choices (Gomes et al., 2011).
378 However, identification of restricted RPC states with limited cell fate potential
379 suggests that there are at least some deterministic processes involved and
380 these are additional, discrete cellular steps in the formation of specific cell
381 types during which genes could act. Here we attempted to integrate the well-
382 documented role for the Notch pathway in the repression of cone
383 photoreceptor formation and promotion of RPC proliferation, within a
384 framework for retinal development that includes restricted RPCs.

385 We initially hypothesized that, similar to other systems, the effect of
386 Notch inhibition on cone photoreceptors would be mediated through sister cell
387 fate decisions. This would be consistent with the fact that there is a restricted
388 RPC type that primarily forms cones and HCs and that several reports that
389 examined the Notch1 mouse mutant identified an increase in cones and one
390 also reported a decrease in HCs. However, though we also detected reduced

391 HCs when we interfered with Notch signaling, we did not detect a concomitant
392 increase in photoreceptors within the ThrbCRM1 restricted RPC daughter cell
393 population. This suggests that sister cell fate choice is not the primary site of
394 functional Notch signaling during cone photoreceptor formation. The most
395 prominent and consistent effects of Notch signaling we observed were on the
396 formation of the ThrbCRM1-active restricted RPC population and a
397 concomitant depletion of the multipotent RPC population, which suggests that
398 the primary role for Notch signaling in cone formation is at the step of
399 restricted RPC derivation from multipotent RPCs. Our interpretation of these
400 results is consistent with another recent developmental study that undertook a
401 comprehensive transcriptome analysis of DAPT-treated embryonic mouse
402 retinas (Kaufman et al., 2019). Here, it was reported that the earliest effects of
403 Notch inhibition through DAPT treatment include the loss of multipotent RPC
404 gene expression (observed as well by earlier studies of Notch1 and Rbpj), but
405 also the early increase of genes that have identified primary correlations with
406 restricted RPCs and with reduced to no expression in postmitotic cones
407 (Jadhav et al., 2006; Riesenberg et al., 2009; Yaron et al., 2006). These gene
408 expression changes include Olig2 (Hafler et al., 2012), Onecut1 (Emerson et
409 al., 2013), and Otx2, all of which have been previously shown to be expressed
410 in restricted RPCs that give rise to cones (Emerson et al., 2013; Hafler et al.,
411 2012). Additional genes such as Dll4 (Rocha et al., 2009), and Atoh7
412 (Buenaventura et al., 2018), are expressed in cycling cells and are enriched in
413 ThrbCRM1 cells as assessed by bulk RNA-Seq. All of these genes displayed
414 a temporal dynamic consistent with increased production of restricted RPCs in
415 this mouse model. In addition, several studies (Kaufman et al., 2019; Nelson
416 et al., 2007) have identified an upregulation of several members of the bHLH
417 family (NeuroD1, Ngn2, etc) which recent single cell analysis has associated
418 with neurogenic RPCs and not multipotent RPCs (Lu et al., 2020).
419 A role for Notch signaling in maintaining a self-renewing multipotent
420 RPC population is also consistent with its observed effects on proliferation.

421 Many studies (Jadhav et al., 2006; Kaufman et al., 2019; Yaron et al., 2006)
422 have identified a decrease in cycling cells when Notch signaling is inhibited.
423 We also detected a significant decrease within two days of electroporation,
424 but consistent with other analysis at early time points in the mouse, there was
425 only a partial loss of cycling cells. Given the identified shift from multipotent to
426 restricted RPCs identified here, we would predict that the majority of the
427 remaining cycling cells in mouse Notch loss-of-function paradigms represent
428 restricted RPCs and that the loss of multipotent RPCs is actually much larger
429 than was assumed to be the case.

430 The evidence presented in the current study, and interpreted from
431 previous ones, suggests a primary role in Notch signaling for mediating the
432 multipotent to restricted RPC transition, but there are critical questions that
433 remain to be addressed. One question is how cell division patterns of
434 multipotent RPCs change with inhibition of Notch signaling? Instead of a
435 multipotent RPC dividing asymmetrically to form another multipotent RPC and
436 a ThrbCRM1 RPC, does Notch inhibition cause symmetrical divisions to form
437 two ThrbCRM1 RPCs? Previous studies have also suggested that there may
438 exist an additional RPC state located between multipotent RPCs and
439 ThrbCRM1 RPCs (Schick et al., 2019; Suzuki et al., 2013). This RPC divides
440 to form an RGC and a ThrbCRM1 RPC on division. The formation of these
441 cells could be the first change elicited by Notch inhibition which would suggest
442 that RGCs should also increase. We do observe a number of cells in the RGC
443 layer, however, we have not detected an increase in RGCs using early RGC
444 markers such as Islet1 and Brn3. It is possible that the continued inhibition of
445 the Notch signaling pathway in these cells interferes with their differentiation.
446 This study focused on the formation of cone photoreceptors, but it will be
447 interesting to determine if Notch functions at other temporal points in
448 retinogenesis to control the formation of other restricted RPC types. Lastly, it
449 will be informative to determine the direct functional targets of Notch signaling
450 that drive RPC transitions. Identification of these pathways will have

451 implications for our understanding of visual system evolution and for the
452 development of strategies to control the proliferation dynamics and cell fate
453 choices of stem cells for therapeutic uses.
454
455 **Methods**
456 **Animals**
457 All experimental procedures involving animals were carried out in consultation
458 with the City College of New York, CUNY Institutional Animal Care protocols.
459 Fertilized chick eggs were acquired from Charles River, stored in a 16 °C
460 room for less than 10 days and incubated in a 38 °C humidified incubator for 5
461 days. All experiments that used animals were not sex-biased.
462
463 **DNA Plasmids**
464 The Hes1 reporter (CBFRE-EGFP) was obtained from Nicholas Gaiano
465 (Addgene plasmid #17705; http://n2t.net/addgene:17705;
466 RRID:Addgene_17705) and described in (Mizutani et al., 2007). The
467 Hes5::GFP reporter was described in (Vilas-Boas et al., 2011). 12XCSL-
468 EGFP reporter (12XCSL-d1EGFP) was obtained from Urban Lendahl
469 (Addgene plasmid # 47684; http://n2t.net/addgene:47684;
470 RRID:Addgene_47684) and described in (Hansson et al., 2006). CAG::βgal
471 was obtained from the Cepko lab (Cepko Lab, Harvard Medical School).
472 CAG::TdT was described in (Schick et al., 2019). OC1ECR22::GFP was
473 described in (Patoori et al., 2020 and manuscript in preparation).
474 VSX2ECR4::GFP reporter and CAG::iRFP were described in (Buenaventura
475 et al., 2018). ThrbCRM1::GFP and ThrbCRM2::GFP reporters were previously
476 reported (Emerson et al., 2013). The lineage trace driver ThrbCRM1::PhiC31
477 and its responder plasmid (CaNa::GFP) were described in (Schick et al.,
478 2019).
479 To make the CAG::MAML-DN plasmid (Addgene plasmid # 160923, this
480 study), an N-terminal MAML coding fragment (Weng et al., 2003) was

481 amplified from chicken cDNA and fused with a mouse Gapdh coding
482 sequence through overlap extension PCR. The PCR product was purified and
483 digested with Age Ⅰ /Nhe Ⅰ before ligation into an Age Ⅰ /Nhe Ⅰ digested
484 CAG::AU1 vector. ThrbCRM1::MAML-DN was made by replacing the CAG
485 promoter with the ThrbCRM1 element. The CAG::Rbpj-EnR (Addgene
486 plasmid # 160924, this study) and CAG::EnR-Rbpj (Addgene plasmid #
487 160925, this study) were made by fusing mouse Rbpj (GenBank ID
488 BC051387.1 obtained from Transomics) with an engrailed repressor domain
489 (Vickers and Sharrocks, 2002) and amplification through overlap extension
490 PCR. The amplicon was digested by EcoR Ⅰ and ligated into an EcoR Ⅰ
491 digested CAG vector. All the plasmids described above were validated by
492 restriction digest and Sanger sequencing.
493
494 **Electroporation and Culture**
495 To deliver plasmid DNA into dissected retinas, *ex vivo* experiments were
496 carried out as described in (Emerson and Cepko, 2011) using a Nepagene
497 NEPA21 Type II Super Electroporator. DNA mixes for *ex vivo* electroporation
498 were made in 1X PBS with a final concentration of 0.1 µg/µl for the co-
499 electroporation control plasmids with CAG promoters and 0.16 µg/µl for
500 reporter and dominant-negative plasmids. Retinas were dissected at E5 and
501 cultured between 8 hours and 2 days after electroporation.
502
503 **Immunohistochemistry**
504 After harvest, retinas were fixed in 4% paraformaldehyde for 30 minutes,
505 washed 3 times in 1XPBS, and sunk in 30% sucrose/0.5XPBS overnight.
506 Retinas were frozen in OCT (Sakura Tissue-Tek, 4583). 20 µm vertical
507 sections were acquired using a Leica Cryostat and collected on 5-7 slides
508 (FisherBrand, 12-550-15).
509 Sections were blocked in 5% serum (Jackson ImmunoResearch, Donkey -
510 017-000121, Goat - 005-000-121) in 1XPBT (0.01% Tween-20 in 1XPBS) for

511 1 hour at room temperature and incubated in primary antibody at 4℃
512 overnight. The primary antibodies used were: chicken anti-GFP (ab13970,
513 Abcam, 1:1000), rabbit anti-GFP (A-6455, Invitrogen, 1:1000), chicken anti-β-
514 galactosidase (ab9361, Abcam, 1:1000), mouse IgG1 anti-β-galactosidase
515 (40-1a-s, DSHB 1:20), rabbit anti-RFP (600-401-379, Rockland, 1:250),
516 mouse IgG1 anti-Visinin (7G4-s, DSHB, 1: 500), mouse IgG1 anti-Lim1 (4F2-
517 c, DSHB, 1:30), mouse anti-AP2α (3B5, DSHB, 1:200), mouse IgG1 anti-
518 Islet1 (39.3F7, DSHB, 1:50), mouse IgG1 anti-Brn3a (MAB1585, EMD
519 Millipore, 1:800), mouse anti-Pan-Brn3 (Sc-390781, Santa Cruz, 1:100),
520 sheep anti-Vsx2 (x1180p, Ex Alpha, 1:200), goat anti-Otx2 (AF1979, R&D,
521 1:500), rabbit anti-Otx2 (AB21990, Abcam, 1:500) and rabbit anti-Olig2
522 (4B9610-AF488, Millipore, 1:500). Sections were washed 3 times with 1XPBT,
523 blocked at room temperature for 30 min and incubated in secondary antibody
524 at 4℃ overnight. The secondary antibodies used were from Jackson
525 Immunoresearch and appropriate for multiple labeling. Alexa 488- and 647-
526 conjugated secondary antibodies (resuspended in 50% glycerol) were used at
527 1:400 and cy3-conjugated antibodies were used at 1:250 as described
528 (Schick et al., 2019). 4'6-diamidino-2-phenylindole (DAPI) was added at 1
529 μg/ml after 3X wash with 1XPBT. Sections were mounted using Fluoromount-
530 G (Southern Biotech, 0100-01) and 34x60 mm coverslips (VWR, 48393-106).
531

532 **EdU Labeling**

533 Before fixation, retinas were incubated at 37℃ for 1 hour with 50 μM EdU in
534 culture media and harvested as described above. Sections were
535 permeabilized for 15 minutes in 0.1% Triton in 1X PBS before incubating with
536 the EdU Reaction Cocktail for 30 minutes in the dark. Sections were washed
537 3 times with 1X PBT before blocking and antibody staining. EdU was detected
538 using a Click-iT EdU Alexa Fluor 647 imaging kit (Invitrogen, C10340).
539

540 **Confocal Microscopy and Cell Counting**

541 Confocal images were acquired using a Zeiss LSM710 inverted confocal
542 microscope with an EC Plan-Neofluar 40x/1.30 Oil DIC M27 immersion
543 objective, 488nm laser, 561 nm laser, 633 nm laser, 405 nm laser, and ZEN
544 Black 2015 21 SP2 software resolution of 1024 x 1024, acquisition speed of 6.
545 Fiji (Schindelin et al., 2012) was used to analyze images and convert into
546 picture format. Cell counting was performed using the Cell Counter plugin-in
547 for ImageJ developed by Kurt De Vos. Cell counts used at least 3 retinas for
548 each condition, 3 technical replicates per retina. Figures were assembled
549 using Affinity Designer vector editor (Serif [Europe] Ltd). Brightness and
550 contrast were adjusted uniformly in all the figures. All retinal sections are
551 oriented with the developing photoreceptor side at the top of the image. All
552 images are presented as maximum projections, with the exception of Olig2-
553 related images in Figure 3A, which are single z-planes.
554

555 **Retinal Cells Dissociation and Flow Cytometry**

556 After ex vivo culture, the remaining retinal pigment epithelium (RPE) and
557 condensed vitreal materials were removed in HBSS (GIBCO, 14170112) and
558 dissociated following a papain-based (Worthington, L5003126) protocol
559 (Jean-Charles et al., 2018). Dissociated retinal cells were fixed using 4%
560 paraformaldehyde for 15 minutes and washed 3 times in 1X PBS. Samples for
561 quantification were filtered into 4ml tubes (BD Falcon, 352054) through 40um
562 cell strainers (Biologix, 15-1040). Dissociated cells were analyzed with a BD
563 LSR II flow cytometer using the 488nm, 561nm, and 633nm lasers. All flow
564 cytometry data was analyzed using FlowJo Version 10.4.2.
565

566 **Statistical Analysis**

567 Graphs and statistical tests were conducted using Microsoft Office Excel and
568 GraphPad Prism 8. The error bars represent S.E.M. ANOVA with a post hoc
569 Dunn test was used in Fig. 4B and Fig. S2B. Mann-Whitney test was used in
570 Fig. 4D, Fig. 5B, Fig 6B, Fig. S4B and Fig. S7B. Student's t-test was used in

the rest of qualifications. All the tests were performed with independent samples after the Shapiro-Wilk normality test using GraphPad Prism8, and the results were significant as noted. Quantifications for flow cytometry were based on 4 biological replicates per condition and at least 2 technical replicates. Quantifications for cell counting were based on 3 biological replicates per condition and at least 3 technical replicates.

Acknowledgements

Funding for this project was provided by NSF CAREER 1453044 (to M.E.) and supported by NIMHD 3G12MD007603-30S2 (to CCNY). Jeffrey Walker and Jorge Morales provided technical support with flow cytometry and confocal microcopy experiments. We thank Diego Buenaventura for providing the VSX2ECR4::PhiC31 plasmid and for guidance with flow cytometry analysis. We thank Miruna Ghinia-Tegla for advice on cell counting and Estie Schick for comments on the manuscript. Shirley Chan, Denice Moran and Boguslava Dimitrova provided technical assistance. We thank all the members of the Emerson lab for support throughout the project.

Author Contributions

XC and ME designed the experiments and analyzed the data. XC and ME conducted the experiments. XC and ME wrote the manuscript.

Competing Interests

The author(s) declare no competing interests.

References

Artavanis-Tsakonas, S., Delidakis, C., and Fehon, R.G. (1991). The Notch locus and the cell biology of neuroblast segregation. Annu. Rev. Cell Biol. *7*, 427–452.

Bray, S. (1998). Notch signalling in Drosophila: three ways to use a pathway. Semin. Cell Dev. Biol. *9*, 591–597.

Bray, S.J. (2006). Notch signalling: a simple pathway becomes complex. Nat. Rev. Mol. Cell Biol. *7*, 678–689.

Buenaventura, D.F., Ghinia-Tegla, M.G., and Emerson, M.M. (2018). Fate-restricted retinal progenitor cells adopt a molecular profile and spatial position distinct from multipotent progenitor cells. Dev. Biol. *443*, 35–49.

Buenaventura, D.F., Corseri, A., and Emerson, M.M. (2019). Identification of Genes With Enriched Expression in Early Developing Mouse Cone Photoreceptors. Invest. Ophthalmol. Vis. Sci. *60*, 2787–2799.

Cepko, C. (2014). Intrinsically different retinal progenitor cells produce specific types of progeny. Nat. Rev. Neurosci. *15*, 615–627.

Emerson, M.M., and Cepko, C.L. (2011). Identification of a retina-specific Otx2 enhancer element active in immature developing photoreceptors. Dev. Biol. *360*, 241–255.

Emerson, M.M., Surzenko, N., Goetz, J.J., Trimarchi, J., and Cepko, C.L. (2013). Otx2 and Onecut1 promote the fates of cone photoreceptors and horizontal cells and repress rod photoreceptors. Dev. Cell *26*, 59–72.

Fischer, A.J., Stanke, J.J., Aloisio, G., Hoy, H., and Stell, W.K. (2007). Heterogeneity of horizontal cells in the chicken retina. J. Comp. Neurol. *500*, 1154–1171.

Ghinia Tegla, M.G., Buenaventura, D.F., Kim, D.Y., Thakurdin, C., Gonzalez, K.C., and Emerson, M.M. OTX2 represses sister cell fate choices in the developing retina to promote photoreceptor specification. ELife *9*.

Gomes, F.L.A.F., Zhang, G., Carbonell, F., Correa, J.A., Harris, W.A., Simons, B.D., and Cayouette, M. (2011). Reconstruction of rat retinal progenitor cell lineages in vitro reveals a surprising degree of stochasticity in cell fate decisions. Dev. Camb. Engl. *138*, 227–235.

Hafler, B.P., Surzenko, N., Beier, K.T., Punzo, C., Trimarchi, J.M., Kong, J.H., and Cepko, C.L. (2012). Transcription factor Olig2 defines subpopulations of retinal progenitor cells biased toward specific cell fates. Proc. Natl. Acad. Sci. *109*, 7882–7887.

632 Hansson, E.M., Teixeira, A.I., Gustafsson, M.V., Dohda, T., Chapman, G.,
633 Meletis, K., Muhr, J., and Lendahl, U. (2006). Recording Notch signaling in real
634 time. Dev. Neurosci. *28*, 118–127.

635 Jadhav, A.P., Mason, H.A., and Cepko, C.L. (2006). Notch 1 inhibits
636 photoreceptor production in the developing mammalian retina. Dev. Camb. Engl.
637 *133*, 913–923.

638 Jean-Charles, N., Buenaventura, D.F., and Emerson, M.M. (2018).
639 Identification and characterization of early photoreceptor cis-regulatory
640 elements and their relation to Onecut1. Neural Develop. *13*, 26.

641 Johnson, J.E., and MacDonald, R.J. (2011). Chapter three - Notch-Independent
642 Functions of CSL. In Current Topics in Developmental Biology, C. Birchmeier,
643 ed. (Academic Press), pp. 55–74.

644 Kaufman, M.L., Park, K.U., Goodson, N.B., Chew, S., Bersie, S., Jones, K.L.,
645 Lamba, D.A., and Brzezinski, J.A. (2019). Transcriptional profiling of murine
646 retinas undergoing semi-synchronous cone photoreceptor differentiation. Dev.
647 Biol. *453*, 155–167.

648 Kopan, R., and Ilagan, M.X.G. (2009). The canonical Notch signaling pathway:
649 unfolding the activation mechanism. Cell *137*, 216–233.

650 Lai, E.C. (2004). Notch signaling: control of cell communication and cell fate.
651 Dev. Camb. Engl. *131*, 965–973.

652 Liu, W., Khare, S.L., Liang, X., Peters, M.A., Liu, X., Cepko, C.L., and Xiang, M.
653 (2000). All Brn3 genes can promote retinal ganglion cell differentiation in the
654 chick. Dev. Camb. Engl. *127*, 3237–3247.

655 Lu, Y., Shiau, F., Yi, W., Lu, S., Wu, Q., Pearson, J.D., Kallman, A., Zhong, S.,
656 Hoang, T., Zuo, Z., et al. (2020). Single-Cell Analysis of Human Retina Identifies
657 Evolutionarily Conserved and Species-Specific Mechanisms Controlling
658 Development. Dev. Cell *53*, 473-491.e9.

659 Mizeracka, K., DeMaso, C.R., and Cepko, C.L. (2013). Notch1 is required in
660 newly postmitotic cells to inhibit the rod photoreceptor fate. Dev. Camb. Engl.
661 *140*, 3188–3197.

662 Mizutani, K., Yoon, K., Dang, L., Tokunaga, A., and Gaiano, N. (2007).
663 Differential Notch signalling distinguishes neural stem cells from intermediate
664 progenitors. Nature *449*, 351–355.

665 Mumm, J.S., and Kopan, R. (2000). Notch signaling: from the outside in. Dev.
666 Biol. *228*, 151–165.

667 Nelson, B.R., Hartman, B.H., Georgi, S.A., Lan, M.S., and Reh, T.A. (2007).
668 Transient inactivation of Notch signaling synchronizes differentiation of neural
669 progenitor cells. Dev. Biol. *304*, 479–498.

670 Patoori, S., Jean-Charles, N., Gopal, A., Sulaiman, S., Gopal, S., Wang, B.,
671 Souferi, B., and Emerson, M.M. (2020). Cis-regulatory analysis of Onecut1
672 expression in fate-restricted retinal progenitor cells. Neural Develop. *15*, 5.

673 Riesenberg, A.N., Liu, Z., Kopan, R., and Brown, N.L. (2009). Rbpj cell
674 autonomous regulation of retinal ganglion cell and cone photoreceptor fates in
675 the mouse retina. J. Neurosci. Off. J. Soc. Neurosci. *29*, 12865–12877.

676 Riesenberg, A.N., Conley, K.W., Le, T.T., and Brown, N.L. (2018). Separate and
677 coincident expression of Hes1 and Hes5 in the developing mouse eye. Dev.
678 Dyn. Off. Publ. Am. Assoc. Anat. *247*, 212–221.

679 Rocha, S.F., Lopes, S.S., Gossler, A., and Henrique, D. (2009). Dll1 and Dll4
680 function sequentially in the retina and pV2 domain of the spinal cord to regulate
681 neurogenesis and create cell diversity. Dev. Biol. *328*, 54–65.

682 Schick, E., McCaffery, S.D., Keblish, E.E., Thakurdin, C., and Emerson, M.M.
683 (2019). Lineage tracing analysis of cone photoreceptor associated cis-
684 regulatory elements in the developing chicken retina. Sci. Rep. *9*, 1–14.

685 Schindelin, J., Arganda-Carreras, I., Frise, E., Kaynig, V., Longair, M., Pietzsch,
686 T., Preibisch, S., Rueden, C., Saalfeld, S., Schmid, B., et al. (2012). Fiji: an
687 open-source platform for biological-image analysis. Nat. Methods *9*, 676–682.

688 Suzuki, S.C., Bleckert, A., Williams, P.R., Takechi, M., Kawamura, S., and Wong,
689 R.O.L. (2013). Cone photoreceptor types in zebrafish are generated by
690 symmetric terminal divisions of dedicated precursors. Proc. Natl. Acad. Sci. U.
691 S. A. *110*, 15109–15114.

692 Tan, G.C., Mazzoni, E.O., and Wichterle, H. (2016). Iterative Role of Notch
693 Signaling in Spinal Motor Neuron Diversification. Cell Rep. *16*, 907–916.

694 Vickers, E.R., and Sharrocks, A.D. (2002). The use of inducible engrailed fusion
695 proteins to study the cellular functions of eukaryotic transcription factors.
696 Methods San Diego Calif *26*, 270–280.

697 Vilas-Boas, F., Fior, R., Swedlow, J.R., Storey, K.G., and Henrique, D. (2011).
698 A novel reporter of notch signalling indicates regulated and random Notch
699 activation during vertebrate neurogenesis. BMC Biol. *9*, 58.

700 Weng, A.P., Nam, Y., Wolfe, M.S., Pear, W.S., Griffin, J.D., Blacklow, S.C., and
701 Aster, J.C. (2003). Growth suppression of pre-T acute lymphoblastic leukemia
702 cells by inhibition of notch signaling. Mol. Cell. Biol. *23*, 655–664.

Wu, L., Aster, J.C., Blacklow, S.C., Lake, R., Artavanis-Tsakonas, S., and Griffin, J.D. (2000). MAML1, a human homologue of Drosophila mastermind, is a transcriptional co-activator for NOTCH receptors. Nat. Genet. *26*, 484–489.

Yaron, O., Farhy, C., Marquardt, T., Applebury, M., and Ashery-Padan, R. (2006). Notch1 functions to suppress cone-photoreceptor fate specification in the developing mouse retina. Dev. Camb. Engl. *133*, 1367–1378.

711 **Figure Legends**

712 **Fig. 1.** CAG::MAML-DN inhibits the expression of the Hes5 Notch reporter
713 **A.** Schematic representation of the electroporation paradigm with plasmids
714 introduced ex vivo into E5 chick retinas, cultured for two days, dissociated into
715 single cells and analyzed by flow cytometry or confocal micrsocopy. A
716 schematic of the MAML dominant-negative construct is shown. **B.** Confocal
717 images of vertically sectioned E5 chick retinas co-electroporated with
718 CAG::Nucßgal, Hes5::GFP Notch reporter, and with or without CAG::MAML-
719 DN and then cultured for two days. The scale bar in the bottom right picture
720 denotes 40 µm and applies to all images. **C.** Flow cytometry dot plots of
721 dissociated chick retinal cells electroporated *ex vivo* at E5 with a co-
722 electroporation control (CAG::iRFP), Hes5::GFP, and with or without
723 CAG::MAML-DN. The bar graph on the right shows the percentage of
724 Hes5::GFP reporter-positive cells within the electroporated population. Each
725 point represents one biological replicate. The Shapiro-Wilk normality test was
726 used to confirm the normal distribution. ** signifies $p<0.01$ with a student's t-
727 test.

728

729 **Fig. 2.** CAG::MAML-DN induced Notch inhibition promotes ThrbCRM1
730 restricted RPC formation
731 **A.** Confocal images of vertically sectioned E5 chick retinas co-electroporated
732 with CAG::Nucßgal, either ThrbCRM1 or VSX2ECR4 GFP reporters, and with
733 or without CAG::MAML-DN and then cultured for two days. The scale bar
734 shown in the bottom right picture denotes 40 µm and applies to all images.
735 **B.** Flow cytometry quantification of the percentage of ThrbCRM1, ThrbCRM2,
736 VSX2ECR4 and OC1ECR22 reporter-positive cells within the CAG::iRFP
737 electroporated population in E5 retinas cultured for two days. Green bars
738 represent control conditions and yellow bars inclusion of the CAG::MAML-DN
739 construct. Each point represents one biological replicate. The Shapiro-Wilk

740 normality test was used to confirm the normal distribution. * signifies p<0.05,
741 ** signifies p<0.01, *** signifies p<0.001 with a student's t-test.
742
743 **Fig. 3.** Effects of CAG::MAML-DN on endogenous retinal markers
744 **A.** Confocal images of vertically sectioned E5 chick retinas co-electroporated
745 with CAG::Nucßgal, and with or without CAG::MAML-DN and then cultured for
746 two days. Sections were immunostained with Otx2 or Olig2 markers
747 (magenta), CAG::Nucßgal (yellow), and nuclei visualized with DAPI. The
748 scale bar in the bottom right picture denotes 40 μm and applies to all images.
749 **B.** Flow cytometry quantification of the percentage of Visinin, Otx2, Lim1 and
750 AP2α -positive cells within the electroporated cells. Dissociated chick retinal
751 cells electroporated *ex vivo* at E5 with the co-electroporation control
752 CAG::TdTomato, under control (green bars) or CAG::MAML-DN (yellow bars)
753 conditions. The retinas were cultured for two days. Each point represents one
754 biological replicate. The Shapiro-Wilk normality test was used to confirm the
755 normal distribution. ** signifies p<0.01, *** signifies p<0.001 with a student's t-
756 test. **C.** Quantification of the percentage of Olig2-positive cells within the
757 electroporated cell population from cell counting. Sectioned chick retinas
758 electroporated *ex vivo* at E5 with the co-electroporation control
759 CAG::Nucßgal. The retinas were cultured for two days. Each point represents
760 one biological replicate. The Shapiro-Wilk normality test was used to confirm
761 the normal distribution. *** signifies p<0.001 with a student's t-test.
762
763 **Fig. 4.** Targeted expression of MAML-DN to cone/HC restricted RPCs does
764 not alter cone formation
765 **A.** Schematic representation of PhiC31 recombinase-based lineage tracing
766 strategy (Schick et al., 2019). **B.** Flow cytometry quantification of the
767 percentage of ThrbCRM1 reporter-positive cells within all the electroporated
768 cells. Dissociated chick retinal cells electroporated *ex vivo* at E5 with the
769 CAG::iRFP co-electroporation control, and with or without CAG::MAML-DN or

770 ThrbCRM1::MAML-DN and cultured for two days. Each point represents one
771 biological replicate. The Shapiro-Wilk normality test was used to confirm the
772 normal distribution. ANOVA with a post hoc Dunn test was used to test
773 significance. ** signifies $p<0.01$, ns signifies $p>0.05$. **C.** Confocal images of
774 vertically sectioned E5 chick retinas co-electroporated with CAG::Nucßgal
775 using ThrbCRM1::MAML-DN lineage trace with a PhiC31 responder plasmid
776 shown in A. The retinas were cultured for two days post-electroporation.
777 Sections were immunostained with Visinin (magenta), CAG::Nucßgal
778 (orange), and nuclei visualized with DAPI. The scale bar in the bottom right
779 picture denotes 40 µm and applies to all images. **D.** Flow cytometry
780 quantification of the percentage of Otx2, Lim1, AP2α, OC1ECR22 and
781 ThrbCRM2 reporter-positive cells within the ThrbCRM1 lineage traced cell
782 population. Dissociated chick retinal cells electroporated *ex vivo* at E5 with the
783 co-electroporation control CAG::TdTomato, ThrbCRM1::PhiC31 and its
784 responder plasmid, and with or without CAG::MAML-DN. The retinas were
785 cultured for two days post-electroporation. Each point represents one
786 biological replicate. The Shapiro-Wilk normality test was used to confirm the
787 normal distribution. Mann-Whitney test was used to test significance in
788 ThrbCRM2 quantification. A student's t-test was used to test significance in
789 the rest of the quantifications. * signifies $p<0.05$, ** signifies $p<0.01$.
790
791 **Fig. 5.** CAG::MAML-DN induced Notch inhibition leads to a shift from
792 multipotent to cone/HC restricted RPCs. **A-E.** Retinas were cultured for two
793 days post-electroporation. **A.** Flow cytometry quantification of the percentage
794 of EdU-positive cells within the electroporated cell population. Dissociated
795 chick retinal cells electroporated *ex vivo* at E5 with the co-electroporation
796 control CAG::TdTomato with or without CAG::MAML-DN. Retinas were pulsed
797 with EdU for 1 hour before harvest. Each point represents one biological
798 replicate. The Shapiro-Wilk normality test was used to confirm the normal
799 distribution. A student's t-test was used to test significance. **B.** Flow cytometry

800 quantification of EdU+ cells positive for VSX2ECR4 or ThrbCRM1 reporters.
801 Dissociated chick retinal cells electroporated *ex vivo* at E5 with
802 VSX2ECR4::GFP and ThrbCRM1::TdTomato. Retinas were pulsed with EdU
803 for 1 hour before harvest. Each point represents one biological replicate. The
804 Shapiro-Wilk normality test was used to confirm the normal distribution. Mann-
805 Whitney test was used to test significance in VSX2ECR4/EdU+ quantification.
806 A student's t-test was used to test significance in ThrbCRM1/EdU+
807 quantification. ** signifies p<0.01. **C.** Flow cytometry quantification of
808 ThrbCRM1 reporter-positive cells that also express VSX2ECR4 reporter and
809 incorporate EdU from dissociated chick retinal cells electroporated *ex vivo* at
810 E5 with VSX2ECR4::GFP and ThrbCRM1::TdTomato. Retinas were pulsed
811 with EdU for 1 hour prior to harvest. Each point represents one biological
812 replicate. The Shapiro-Wilk normality test was used to confirm the normal
813 distribution. *** signifies p<0.001 with a student's t-test. **D.** Confocal images of
814 vertically sectioned E5 chick retinas co-electroporated with CAG::Nucßgal,
815 ThrbCRM1::GFP or VSX2ECR4::GFP, and with or without CAG::MAML-DN.
816 Retinas were pulsed with EdU for 1 hour before harvest. The scale bar in the
817 bottom right picture denotes 40 μm and applies to all images. **E.** Flow
818 cytometry quantification of the percentage of VSX2ECR4/ThrbCRM1 double
819 reporter-positive cells within the VSX2ECR4 lineage traced population.
820 Dissociated chick retinal cells electroporated *ex vivo* at E5 with the co-
821 electroporation control CAG::iRFP, VSX2ECR4::PhiC31 and its responder
822 plasmid, and with or without CAG::MAML-DN. Each point represents one
823 biological replicate. The Shapiro-Wilk normality test was used to confirm the
824 normal distribution. ** signifies p<0.01 with a student's t-test.
825
826 **Fig. 6.** The short-term effects of Notch inhibition on RPC reporters
827 **A.** Confocal images of vertically sectioned E5 chick retinas co-electroporated
828 with CAG::Nucßgal, ThrbCRM1::GFP or VSX2ECR4::GFP, and with or
829 without CAG::MAML-DN. The retinas were cultured for 8 hours post-

830 electroporation. The scale bar in the bottom right picture denotes 40 μm and
831 applies to all images. **B.** Flow cytometry quantification of the percentage of
832 VSX2ECR4, ThrbCRM1 and VSX2ECR4/ThrbCRM1 reporter-positive cells
833 within all the electroporated cells. Dissociated chick retinal cells
834 electroporated *ex vivo* at E5 with the co-electroporation control CAG::iRFP
835 with or without CAG::MAML-DN. Retinas were cultured for 8 hours post-
836 electroporation. Each point represents one biological replicate. The Shapiro-
837 Wilk normality test was used to confirm the normal distribution. Mann-Whitney
838 test was used to test significance in VSX2ECR4 quantification. A student's t-
839 test was used to test significance in ThrbCRM1 and double-positive
840 quantifications. **C.** Flow cytometry quantification of the percentage of
841 VSX2ECR4, ThrbCRM1 and VSX2ECR4/ThrbCRM1 reporter-positive cells
842 within all the electroporated cells. Dissociated chick retinal cells
843 electroporated with CAG::iRFP *ex vivo* at E5 and cultured for 20 hours. Each
844 point represents one biological replicate. The Shapiro-Wilk normality test was
845 used to confirm the normal distribution. *** signifies $p<0.001$ with a student's t-
846 test. **D.** Quantification of the percentage of VSX2, Otx2 and double marker-
847 positive cells within the electroporated cell population from cell counting.
848 Sectioned chick retinas electroporated *ex vivo* at E5 with the co-
849 electroporation control CAG::Nucßgal with or without CAG::MAML-DN. The
850 retinas were cultured for 20 hours and immunostained with VSX2 or Otx2
851 antibodies. Each point represents one biological replicate. The Shapiro-Wilk
852 normality test was used to confirm the normal distribution. * signifies $p<0.05$,
853 *** signifies $p<0.001$ with a student's t-test.
854
855 **Fig. 7.** Notch inhibition leads to a delayed increase in cones relative to
856 cone/HC RPCs
857 **A.** Schematic of experimental set-up. Retinas were electroporated with
858 VSX2ECR4::PhiC31 and CAG::stopGFP responder plasmid to label
859 multipotent RPCs (mpRPC)s and their progeny. In addition, ThrbCRM2::TdT

860 was co-electroporated to identify a subset of cones. CAG::MAML-DN was
861 included in experimental conditions and omitted in control conditions.
862 CAG::iRFP was included as a co-electroporation control (not shown). Retinas
863 were assessed 2 to 5 days later by flow cytometry to measure GFP, TdT, and
864 iRFP activity. Non-electroporated cells are shown in blue, lineage-traced cells
865 in green, non-lineage traced ThrbCRM2+ cells in magenta and lineage traced
866 ThrbCRM2+ cells in orange. **B.** Flow cytometry quantification of the
867 percentage of ThrbCRM2 reporter-positive cells within all the electroporated
868 cells using VSX2ECR4 lineage trace strategy with the PhiC31 responder
869 plasmid shown in 4A. Dissociated chick retinal cells electroporated *ex vivo* at
870 E5 with the co-electroporation control CAG::iRFP, VSX2ECR4::PhiC31 and its
871 responder plasmid, ThrbCRM2::TdTomato, and with or without CAG::MAML-
872 DN. Retinas were cultured for 2 or 3 days post-electroporation. A student's t-
873 test was used to test significance. Each point represents one biological
874 replicate. The Shapiro-Wilk normality test was used to confirm the normal
875 distribution. * signifies $p<0.05$, ** signifies $p<0.01$, *** signifies $p<0.001$ with a
876 student's t-test. **C.** Same as A but with 4 or 5 days culture.
877
878 **Fig. 8.** Model of Notch inhibition effects on cone/HC regulatory network
879 Schematic of the general relationship between multipotent RPCs (mpRPC,
880 beige), cone/HC RPCs (green), cones (blue), and HCs (purple). Grey shading
881 denotes cell-type limits of Notch inhibition. CAG::MAML-DN is broadly active
882 in all cells (denoted by grey shading) and leads to reduction in mpRPCs,
883 increase in cone/HC RPCs and cones. Bottom graphs represent relative
884 numbers of cell type populations under control and Notch inhibition conditions.
885 Dotted lines depict the control levels of cones and HCs.
886
887 **Fig. S1.** CAG::MAML-DN effects on Hes1 and 12XCSL-EGFP reporters.
888 **A.** Confocal images of vertically sectioned E5 chick retinas co-electroporated
889 with CAG::Nucßgal, Hes1::GFP or 12XCSL-EGFP, and with or without

890 CAG::MAML-DN and cultured for two days. The scale bar in the bottom right
891 picture denotes 40 μm and applies to all images. **B.** Bar graphs of flow
892 cytometry analysis of dissociated chick retinal cells electroporated *ex vivo* at
893 E5 with the CAG::iRFP co-electroporation control, Hes1::GFP reporter (left
894 graph) or 12XCSL-EGFP (right graph), and with or without CAG::MAML-DN
895 and cultured for two days. The number of EGFP reporter-positive cells within
896 the electroporated population is plotted. Each point represents one biological
897 replicate. The Shapiro-Wilk normality test was used to confirm the normal
898 distribution. * signifies $p<0.05$ with a student's t-test.
899
900 **Fig. S2.** Rbpj-EnR has similar effects as CAG::MAML-DN on Hes5 Notch
901 reporter and ThrbCRM1-marked RPCs
902 **A.** Confocal images of vertically sectioned E5 chick retinas co-electroporated
903 with CAG::Nucßgal, Hes5::GFP Notch reporter, and with or without Rbpj-EnR
904 and cultured for two days before Visinin immunostaining. The scale bar in the
905 bottom right picture denotes 40 μm and applies to all images. **B.** Flow
906 cytometry quantification of the percentage of Hes5 and ThrbCRM1-positive
907 cells within all the electroporated cells. Dissociated chick retinal cells
908 electroporated *ex vivo* at E5 with the CAG::iRFP co-electroporation control,
909 Hes5 or ThrbCRM1 reporters, and with or without EnR-Rbpj or Rbpj-EnR and
910 cultured for two days. Each point represents one biological replicate. The
911 Shapiro-Wilk normality test was used to confirm the normal distribution.
912 ANOVA with a post hoc Dunn test was used to test significance. *** signifies
913 $p<0.001$.
914
915 **Fig. S3.** CAG::MAML-DN does not promote cone formation at two days post-
916 electroporation
917 Confocal images of vertically sectioned E5 chick retinas co-electroporated
918 with CAG::Nucßgal, ThrbCRM2::GFP, OC1ECR22::GFP or ThrbCRM1::GFP ,
919 and with or without CAG::MAML-DN and cultured for two days. LHX4 antibody

920 was used to label cones. The scale bar in the bottom right picture denotes 40
921 μm and applies to all images.
922
923 **Fig. S4.** CAG::MAML-DN does not shift the number of H2, H3 and H4 HCs
924 and RGCs. **A.** Confocal images of vertically sectioned E5 chick retinas co-
925 electroporated with CAG::Nucßgal, and with or without CAG::MAML-DN and
926 cultured for two days. Sections were immunostained with Islet1 and Pan-Brn3
927 cell specific markers (magenta), CAG::Nucßgal (orange), and nuclei
928 visualized with DAPI. The scale bar in the bottom right panel denotes 40 μm
929 and applies to all images. **B.** Flow cytometry quantification of the percentage
930 of Islet1, Brn3a and Pan-Brn3-positive cells within all electroporated cells.
931 Dissociated chick retinal cells electroporated *ex vivo* at E5 with the
932 CAG::TdTomato co-electroporation control and cultured for two days. Each
933 point represents one biological replicate. The Shapiro-Wilk normality test was
934 used to confirm the normal distribution. A student's t-test was used to test
935 significance in Islet1 and Brn3a quantifications. Mann-Whitney test was used
936 to test significance in Pan-Brn3 quantification.
937
938 **Fig. S5.** Rbpj-EnR promotes ThrbCRM1 RPCs and represses HCs
939 Flow cytometry quantification of the percentage of VSX2ECR4, ThrbCRM1,
940 VSX2ECR4/ThrbCRM1 double reporter-positive, Visinin, ThrbCRM2, OC-
941 ECR22, Lim1 and AP2α -positive cells within all the electroporated cells.
942 Dissociated chick retinal cells electroporated *ex vivo* at E5 with the
943 CAG::iRFP or CAG::TdTomato co-electroporation control, and with or without
944 Rbpj-EnR and cultured for two days. Each point represents one biological
945 replicate. The Shapiro-Wilk normality test was used to confirm the normal
946 distribution. ** signifies $p<0.01$, *** signifies $p<0.001$ with a student's t-test.
947
948 **Fig. S6.** ThrbCRM1::MAML-DN does not have effects on H2, H3 and H4 HCs
949 and RGCs within ThrbCRM1 lineage traced population

950 **A.** Confocal images of vertically sectioned E5 chick retinas co-electroporated
951 with CAG::Nucßgal, ThrbCRM1::PhiC31 and its responder plasmid, and with
952 or without ThrbCRM1::MAML-DN. The retinas were cultured for two days
953 post-electroporation. The sections were immunostained with Otx2, Lim1 and
954 AP2α markers (magenta), CAG::Nucßgal (orange), and nuclei visualized
955 with DAPI. The scale bar in the bottom right picture denotes 40 μm and
956 applies to all images. **B.** Quantification of the percentage of Islet1 and Brn3
957 marker-positive cells within the ThrbCRM1 lineage traced cell population from
958 cell counting. Sectioned chick retinas electroporated *ex vivo* at E5 with the co-
959 electroporation control CAG::Nucßgal, ThrbCRM1::PhiC31 and its responder
960 plasmid, and with or without ThrbCRM1::MAML-DN. The retinas were cultured
961 for two days after electroporation. Each point represents one biological
962 replicate. The Shapiro-Wilk normality test was used to confirm the normal
963 distribution. A student's t-test was used to test significance.
964
965 **Fig. S7.** Rbpj-EnR induced Notch inhibition has similar effects as
966 CAG::MAML-DN on cell proliferation
967 **A.** Flow cytometry quantification of the percentage of EdU-positive cells within
968 all the electroporated cells. Dissociated chick retinal cells electroporated *ex*
969 *vivo* at E5 with the co-electroporation control CAG::TdTomato with or without
970 Rbpj-EnR. The retinas were cultured for two days after electroporation and
971 pulsed with EdU for 1 hour before harvest. Each point represents one
972 biological replicate. The Shapiro-Wilk normality test was used to confirm the
973 normal distribution. A student's t-test was used to test significance. **B.** Flow
974 cytometry quantification of the percentage of VSX2ECR4, ThrbCRM1 or
975 VSX2ECR4/ThrbCRM1-positive cells within the electroporated cell population.
976 Dissociated chick retinal cells electroporated *ex vivo* at E5 with the co-
977 electroporation control CAG::iRFP, VSX2ECR4::GFP or ThrbCRM1::GFP,
978 and with or without Rbpj-EnR. The retinas were cultured for 8 hours post-
979 electroporation. Each point represents one biological replicate. The Shapiro-

980 Wilk normality test was used to confirm the normal distribution. A student's t-
981 test was used to test significance in ThrbCRM1 quantification. Mann-Whitney
982 test was used to test significance in VSX2ECR4 and double reporter-positive
983 quantifications. * signifies $p<0.05$.
984
985 **Fig. S8.** CAG::MAML-DN induced Notch inhibition led to a transition from
986 VSX2+/EdU+ cells to Otx2+/EdU+ cells
987 Confocal images of vertically sectioned E5 chick retinas co-electroporated
988 with CAG::Nucßgal and with or without CAG::MAML-DN. The retinas were
989 cultured for two days after electroporation and pulsed with EdU for 1 hour
990 before harvest. The sections were immunostained with VSX2 and Otx2
991 makers (magenta), CAG::Nucßgal (orange), and nuclei visualized with DAPI.
992 The scale bar in the bottom right picture denotes 40 μm and applies to all
993 images.

Fig. 1

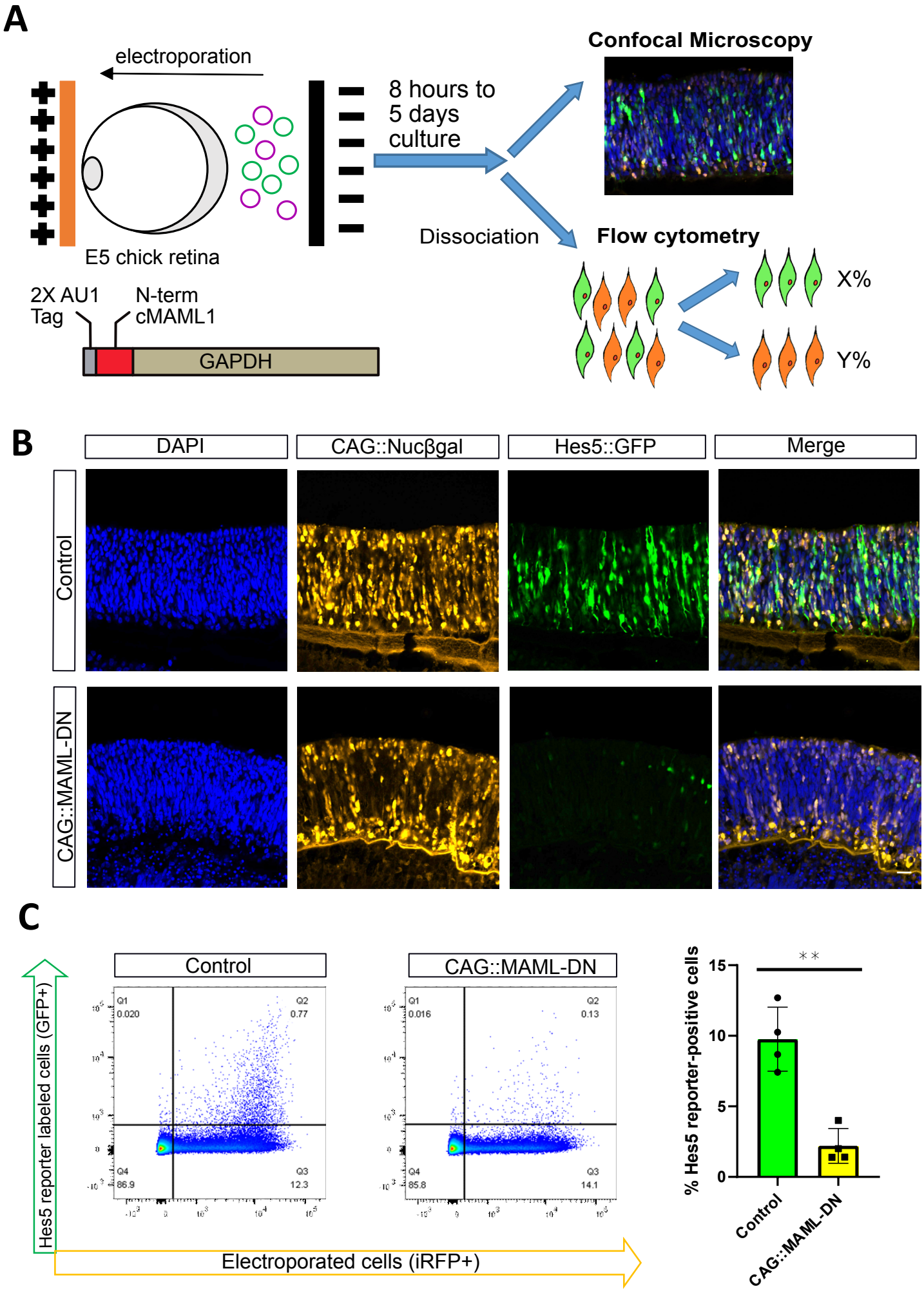
A
electroporation
E5 chick retina
2X AU1 Tag
N-term cMAML1
GAPDH
8 hours to 5 days culture
Dissociation
Confocal Microscopy
Flow cytometry
X%
Y%
B
DAPI
CAG::Nucβgal
Hes5::GFP
Merge
Control
CAG::MAML-DN
C
Control
CAG::MAML-DN
Q1 0.020
Q2 0.77
Q4 86.9
Q3 12.3
Q1 0.016
Q2 0.13
Q4 85.8
Q3 14.1
Hes5 reporter labeled cells (GFP+)
Electroporated cells (iRFP+)
% Hes5 reporter-positive cells
15
10
5
0
**
Control
CAG::MAML-DN

Fig. 2

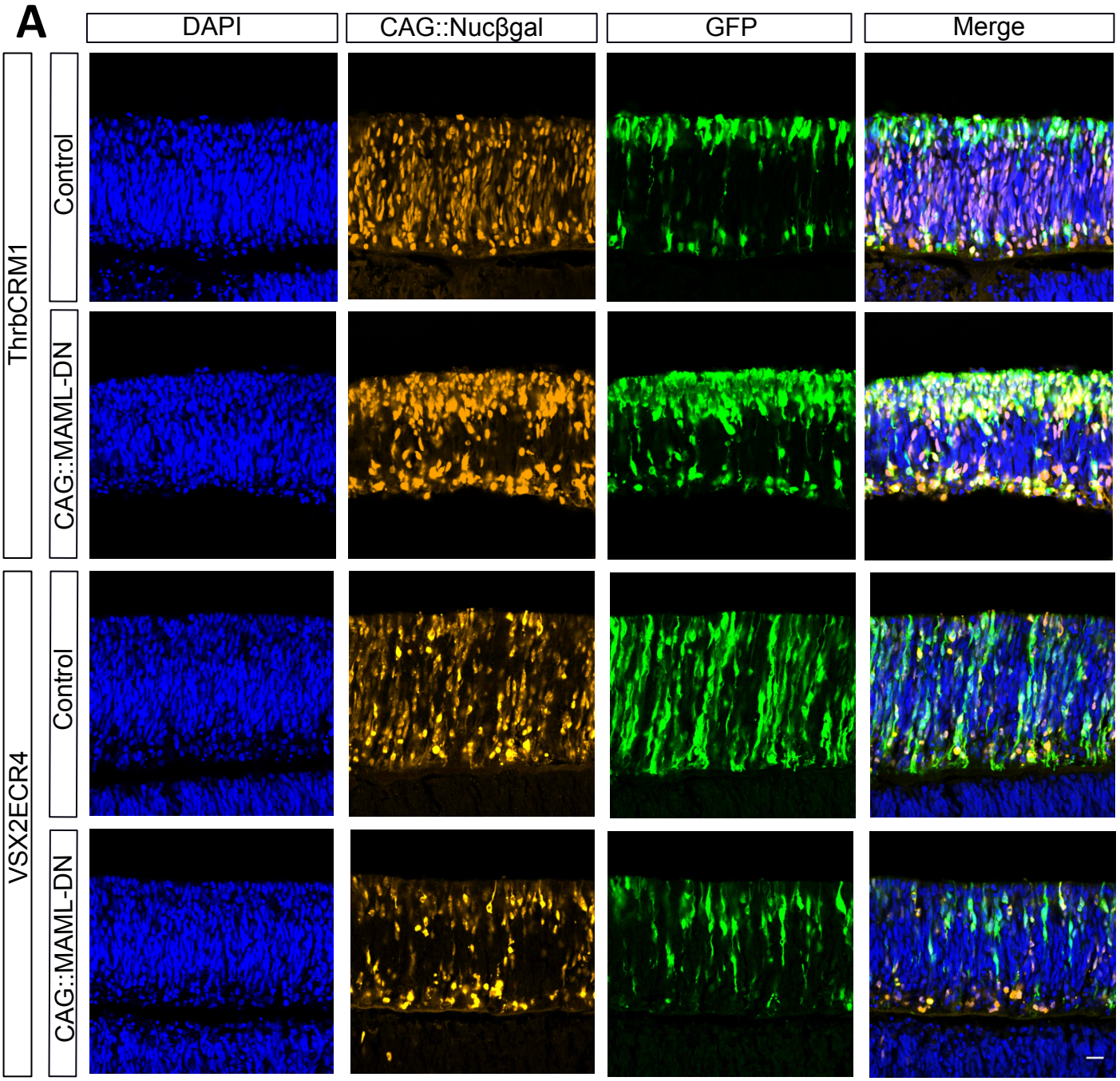
A
DAPI
CAG::Nucβgal
GFP
Merge
ThrbCRM1
Control
CAG::MAML-DN
VSX2ECR4
Control
CAG::MAML-DN

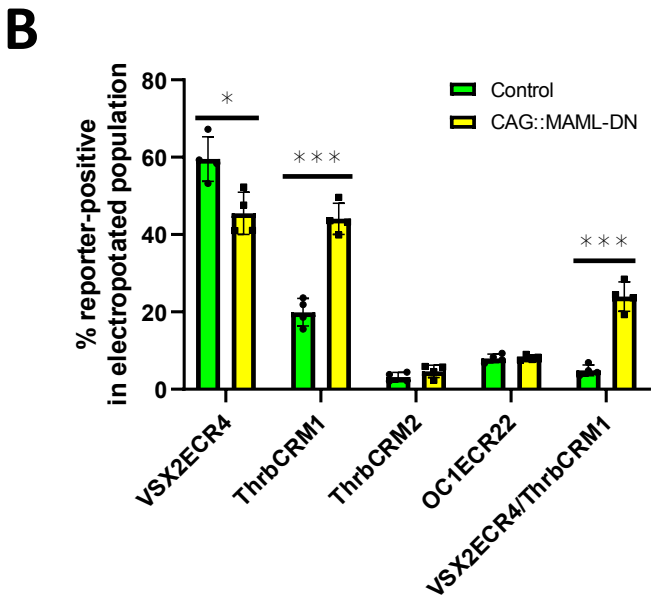
B
% reporter-positive in electropotated population
80
60
40
20
0
Control
CAG::MAML-DN
*
***
***
VSX2ECR4
ThrbCRM1
ThrbCRM2
OC1ECR22
VSX2ECR4/ThrbCRM1

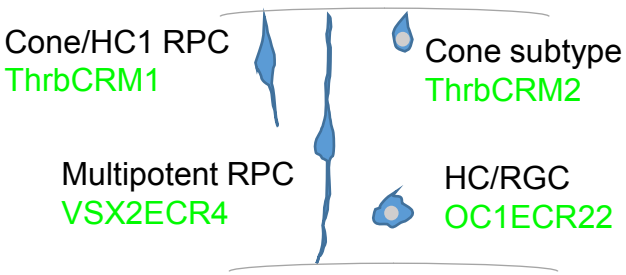
Cone/HC1 RPC
ThrbCRM1
Cone subtype
ThrbCRM2
Multipotent RPC
VSX2ECR4
HC/RGC
OC1ECR22

Fig. 3

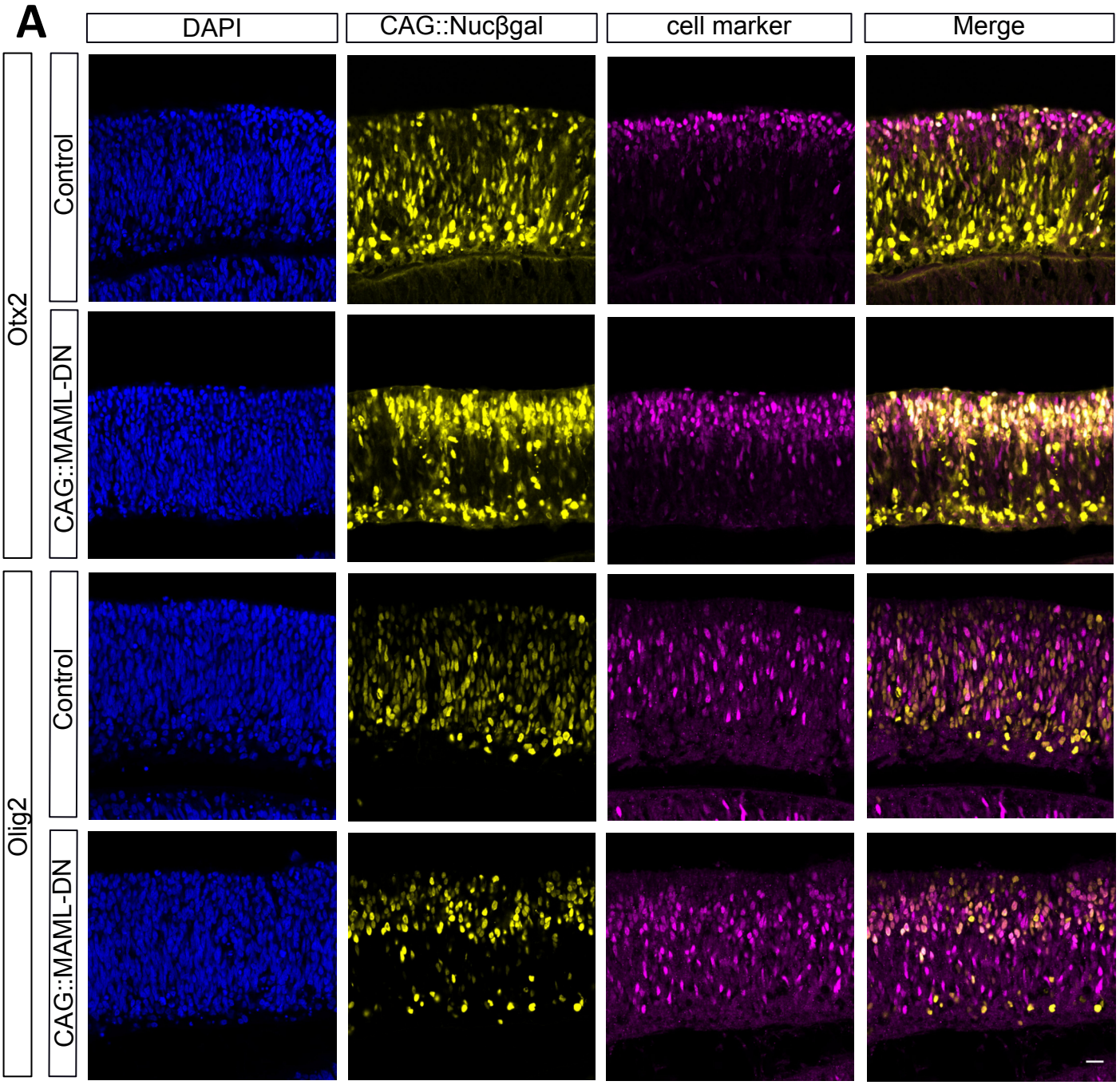
A
DAPI
CAG::Nucβgal
cell marker
Merge
Otx2
Control
CAG::MAML-DN
Olig2
Control
CAG::MAML-DN

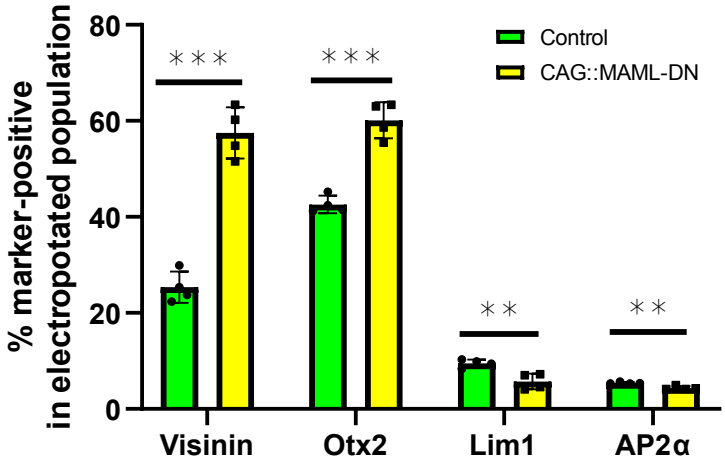
B
% marker-positive
in electropotated population
80
60
40
20
0
***
***
**
**
Control
CAG::MAML-DN
Visinin
Otx2
Lim1
AP2α

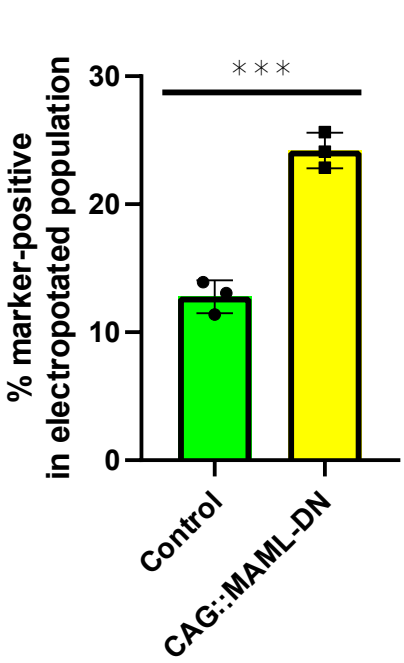
C
% marker-positive
in electropotated population
30
20
10
0
***
Control
CAG::MAML-DN

Fig. 4

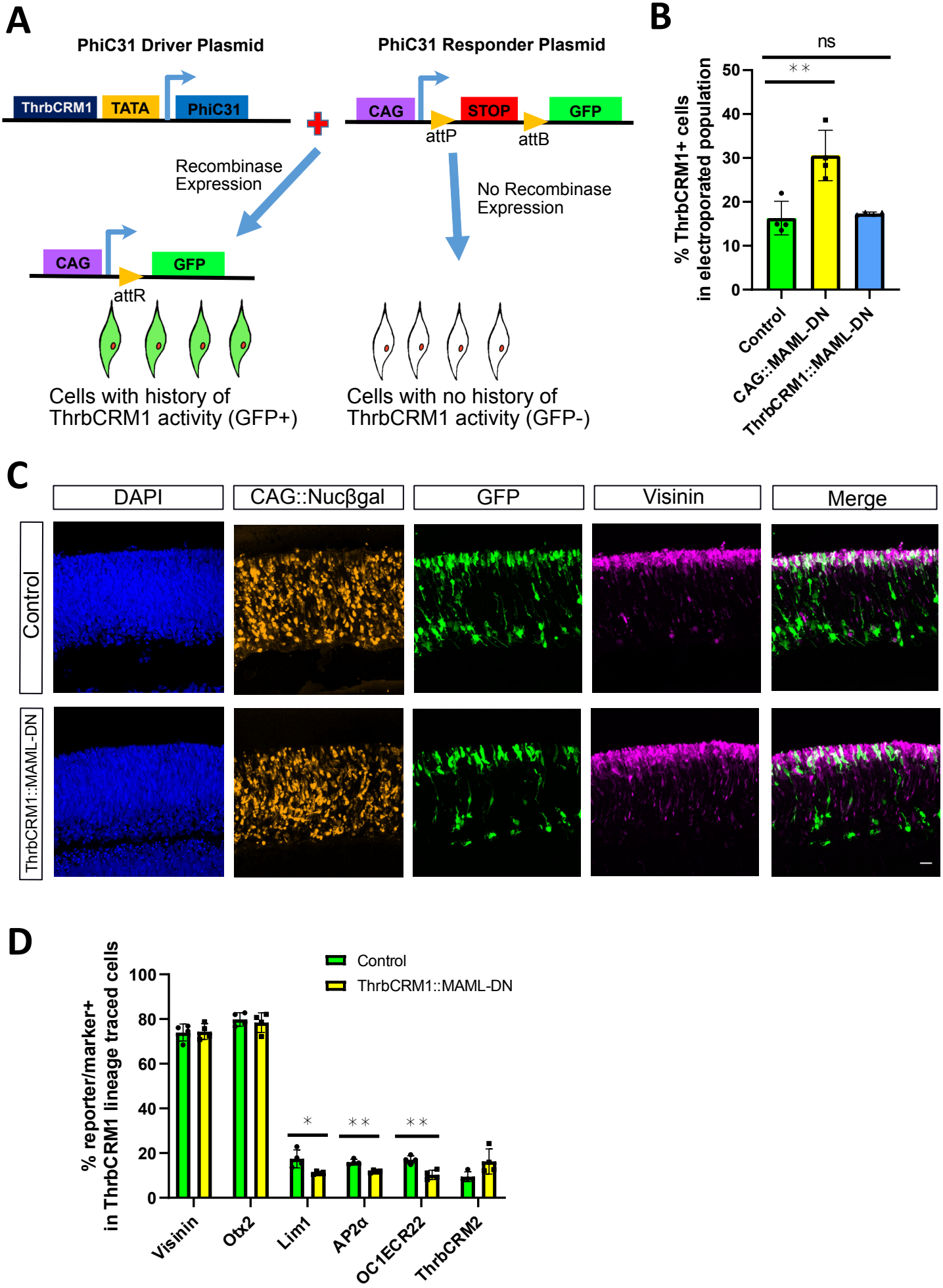
A
PhiC31 Driver Plasmid
ThrbCRM1
TATA
PhiC31
PhiC31 Responder Plasmid
CAG
STOP
GFP
attP
attB
Recombinase Expression
No Recombinase Expression
CAG
GFP
attR
Cells with history of ThrbCRM1 activity (GFP+)
Cells with no history of ThrbCRM1 activity (GFP-)
B
ns
**
% ThrbCRM1+ cells in electroporated population
50
40
30
20
10
0
Control
CAG::MAML-DN
ThrbCRM1::MAML-DN
C
DAPI
CAG::Nucβgal
GFP
Visinin
Merge
Control
ThrbCRM1::MAML-DN
D
Control
ThrbCRM1::MAML-DN
% reporter/marker+ in ThrbCRM1 lineage traced cells
100
80
60
40
20
0
*
**
**
Visinin
Otx2
Lim1
AP2α
OC1ECR22
ThrbCRM2

Fig. 5

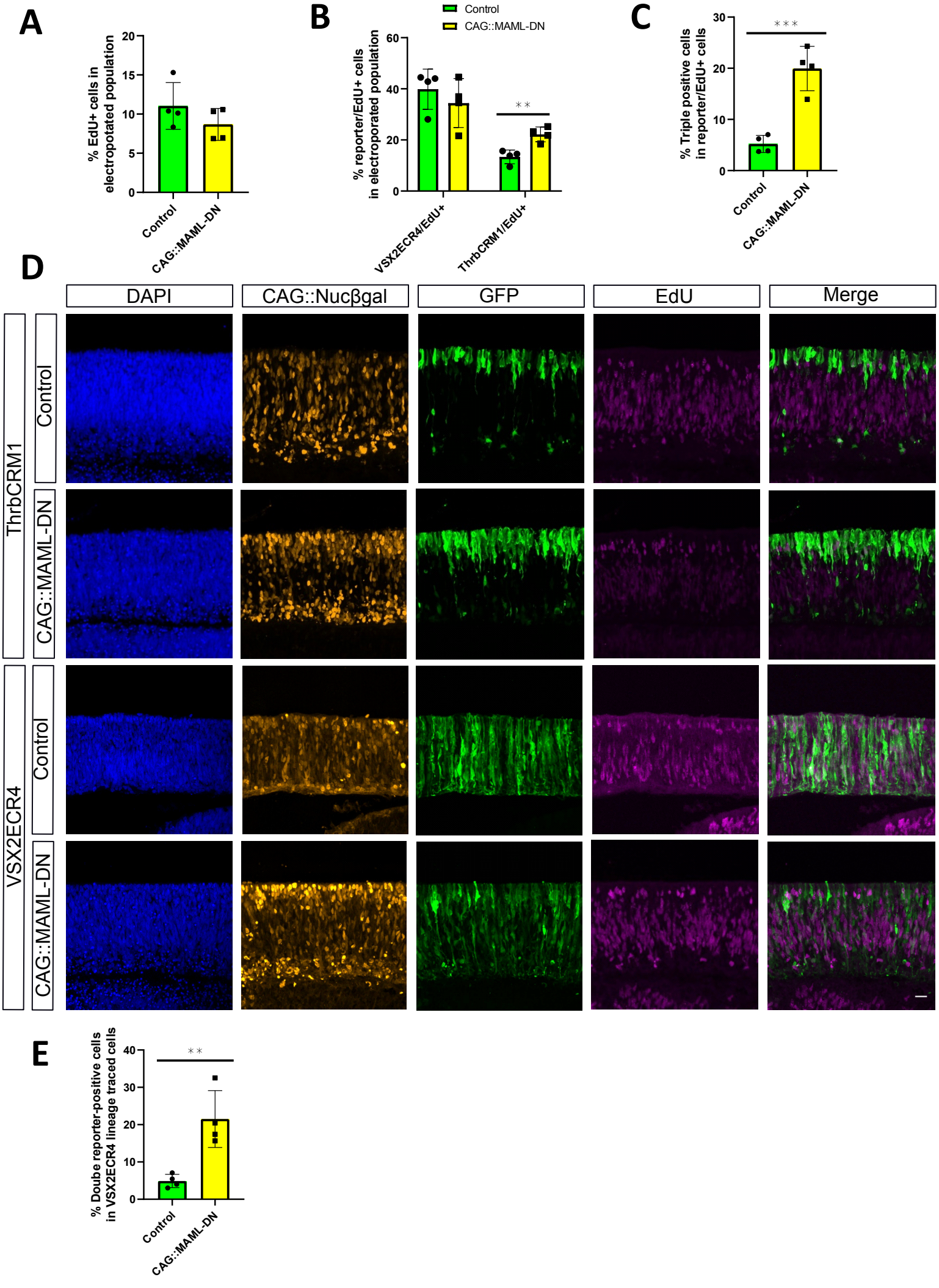
A
% EdU+ cells in electropotated population
20
15
10
5
0
Control
CAG::MAML-DN
B
Control
CAG::MAML-DN
% reporter/EdU+ cells in electroporated population
60
40
20
0
**
VSX2ECR4/EdU+
ThrbCRM1/EdU+
C
% Triple positive cells in reporter/EdU+ cells
30
20
10
0
***
Control
CAG::MAML-DN
D
DAPI
CAG::Nucβgal
GFP
EdU
Merge
ThrbCRM1
Control
CAG::MAML-DN
VSX2ECR4
Control
CAG::MAML-DN
E
% Doube reporter-positive cells in VSX2ECR4 lineage traced cells
40
30
20
10
0
**
Control
CAG::MAML-DN

Fig. 6

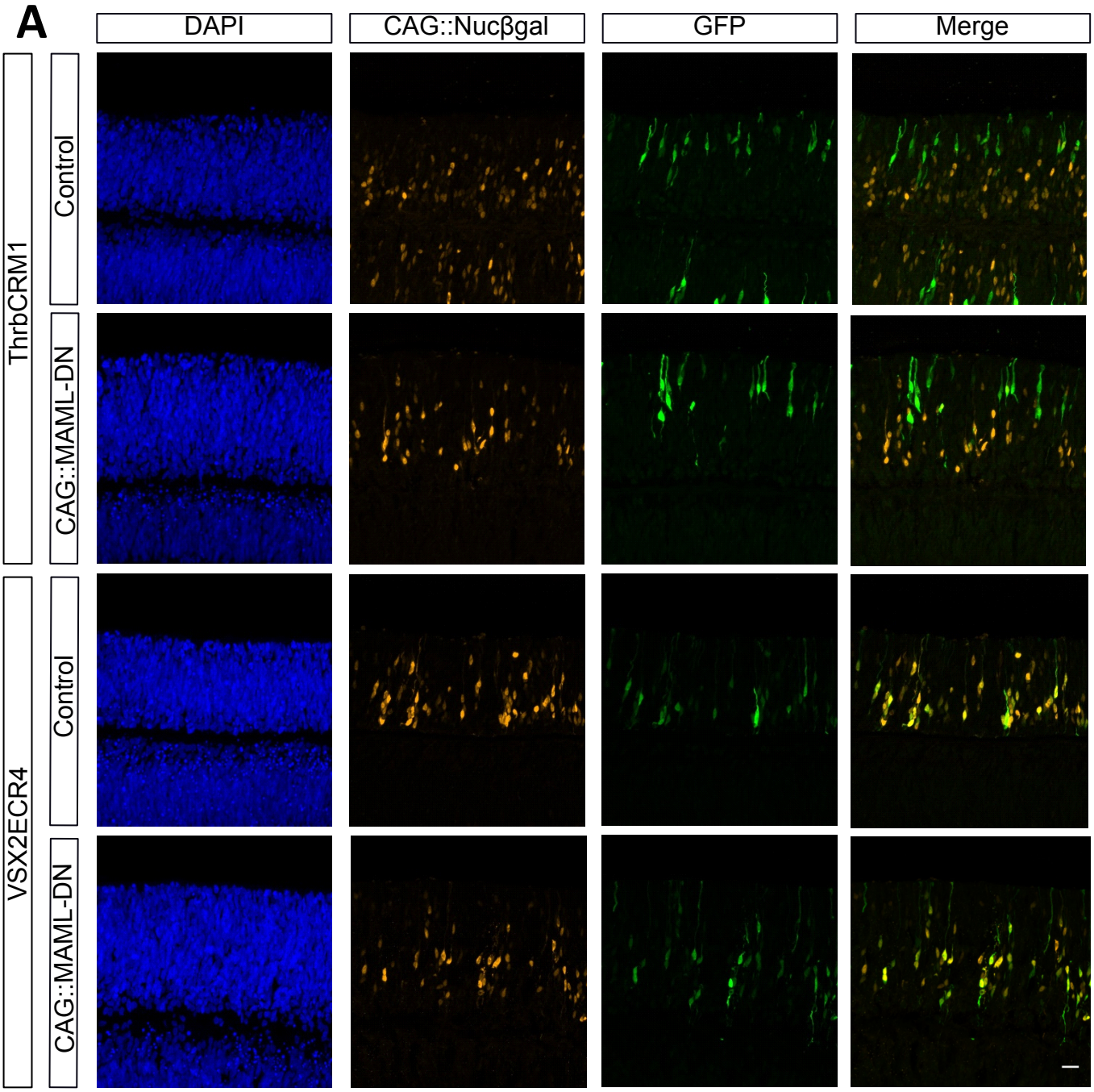
A
DAPI
CAG::Nucβgal
GFP
Merge
ThrbCRM1
Control
CAG::MAML-DN
VSX2ECR4
Control
CAG::MAML-DN

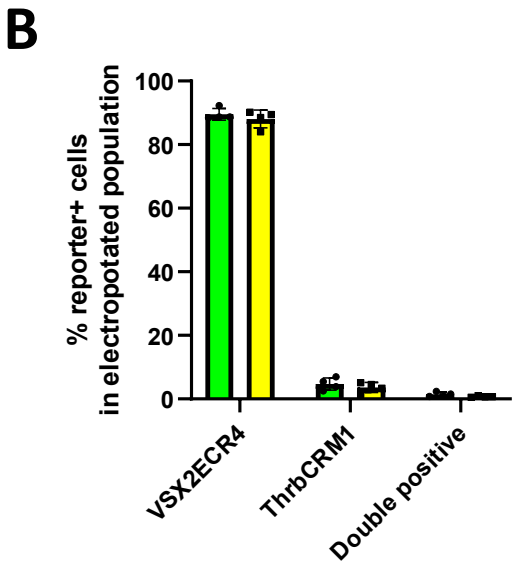
B
% reporter+ cells in electropotated population
100
80
60
40
20
0
VSX2ECR4
ThrbCRM1
Double positive

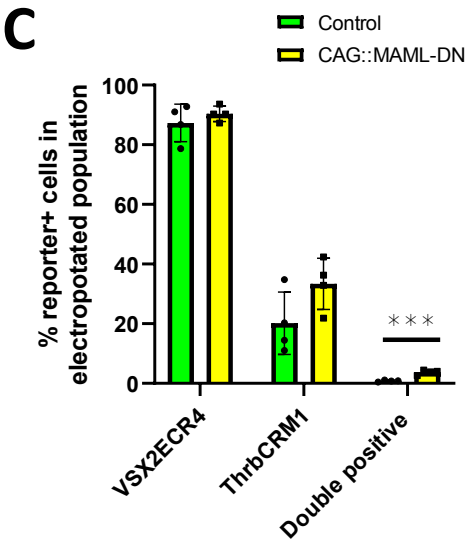
C
Control
CAG::MAML-DN
% reporter+ cells in electropotated population
100
80
60
40
20
0
***
VSX2ECR4
ThrbCRM1
Double positive

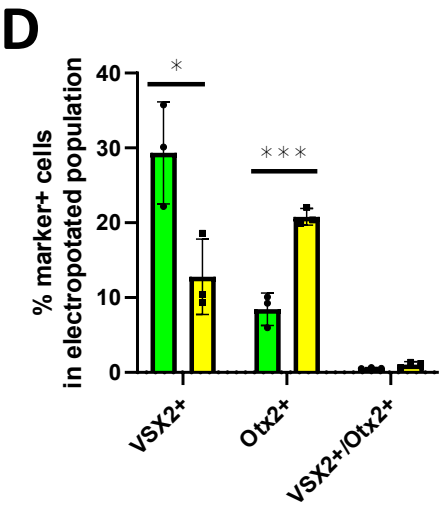
D
% marker+ cells in electropotated population
40
30
20
10
0
*
***
VSX2+
Otx2+
VSX2+/Otx2+

Fig. 7

A

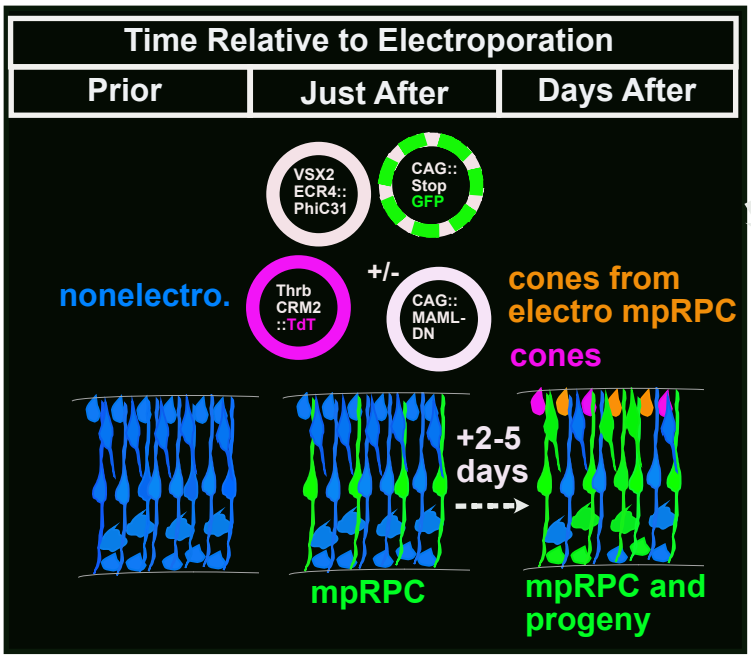
Time Relative to Electroporation
Prior
Just After
Days After
VSX2 ECR4:: PhiC31
CAG:: Stop GFP
nonelectro.
Thrb CRM2 ::TdT
+/-
CAG:: MAML-DN
cones from electro mpRPC
cones
+2-5 days
mpRPC
mpRPC and progeny

B

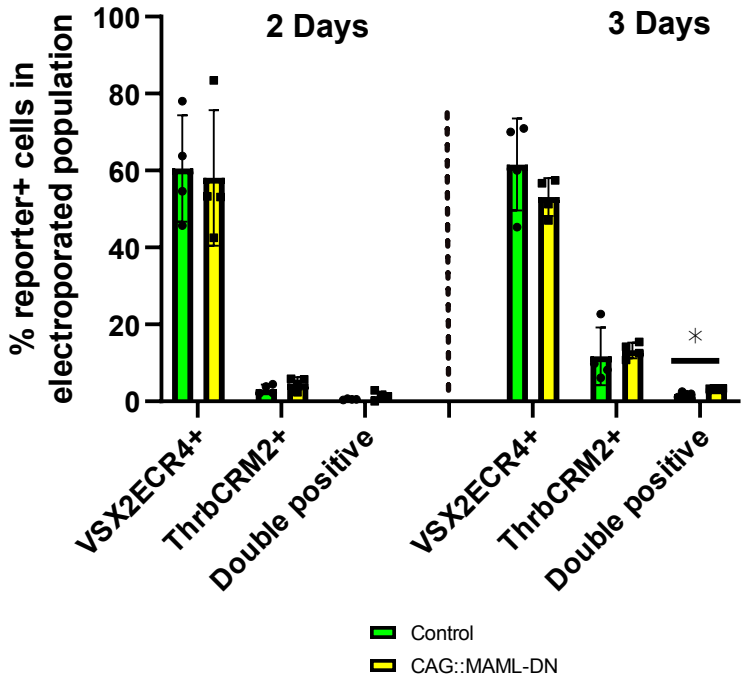
% reporter+ cells in electroporated population
100
80
60
40
20
0
2 Days
3 Days
*
VSX2ECR4+
ThrbCRM2+
Double positive
VSX2ECR4+
ThrbCRM2+
Double positive
Control
CAG::MAML-DN

C

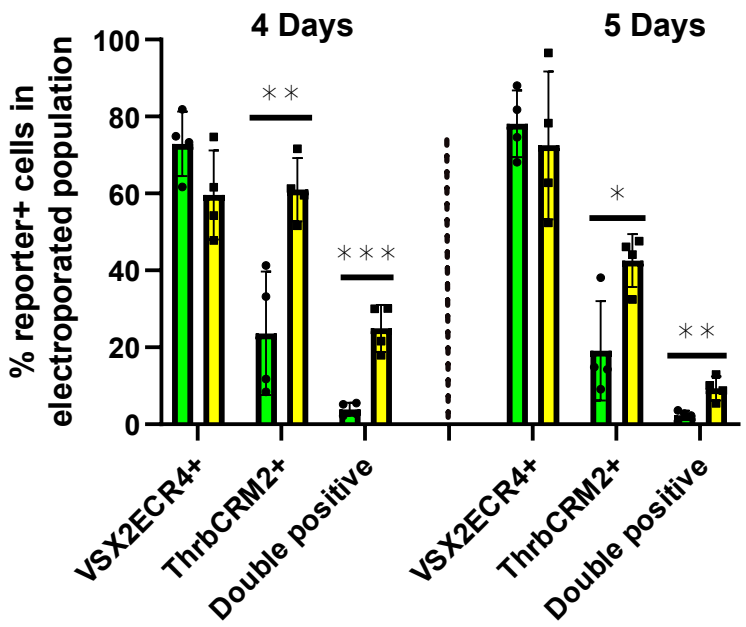
% reporter+ cells in electroporated population
100
80
60
40
20
0
4 Days
5 Days
**
***
*
**
VSX2ECR4+
ThrbCRM2+
Double positive
VSX2ECR4+
ThrbCRM2+
Double positive

Fig.8

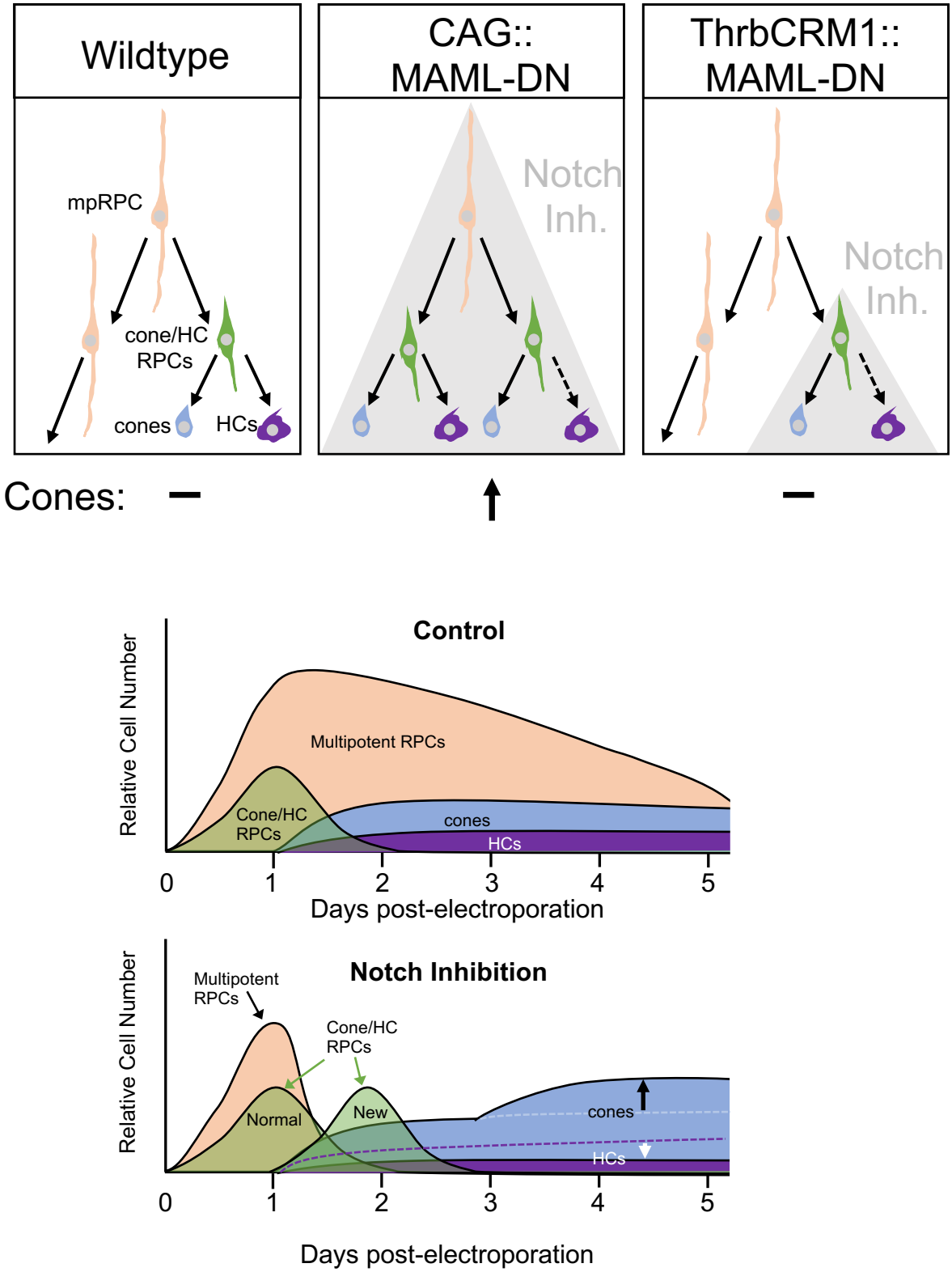
Wildtype
CAG::
MAML-DN
ThrbCRM1::
MAML-DN
mpRPC
cone/HC
RPCs
cones
HCs
Notch
Inh.
Notch
Inh.
Cones:
Control
Relative Cell Number
Multipotent RPCs
Cone/HC
RPCs
cones
HCs
0
1
2
3
4
5
Days post-electroporation
Notch Inhibition
Relative Cell Number
Multipotent
RPCs
Cone/HC
RPCs
Normal
New
cones
HCs
0
1
2
3
4
5
Days post-electroporation